Superradiant clock laser on an optical lattice

Masterarbeit

zur Erlangung des akademischen Grades
Master of Science (MSc.)

eingereicht an der
Fakultät für Mathematik, Informatik und Physik
der Universität Innsbruck

von

Thomas Maier, BSc.

Betreuer:
Prof. Dr. Helmut Ritsch,
Institut für Theoretische Physik

Innsbruck, Juni 2014

Abstract

An almost light less laser[1] - this way Vladan Vuletic describes the concept of a superradiant laser. What sounds a little bit confusing, should build the basis for a new kind of a ultra frequency-stable laser.

An ideal superradiant laser operating on an optical clock transition of a noninteracting ensemble of cold trapped atoms is predicted to exhibit extreme frequency stability and accuracy even far below mHz linewidth. In any concrete setup a sufficiently large number of atoms have to be confined and optically pumped within an optical cavity. Using a magic wavelength lattice minimizes light shifts and allows almost uniform collective coupling to the cavity mode. Nevertheless, the atoms will also be subject to dipole-dipole interaction and undergo collective spontaneous decay limiting the ultimate frequency stability of the device. In the high density limit the Dicke superradiant linewidth enhancement, which is directly proportional to the atom number, broadens the laser line and nearest neighbor couplings will induce line shifts and fluctuations of the absolute laser frequency. We estimate the magnitude and scaling of these effects by direct numerical simulations of few atom systems for different geometries and various densities. Fortunately, for Strontium in a regularly filled magic wavelength configuration, dipole-dipole interaction is small and the suppression of collective spontaneous emission can lead to subradiant line narrowing in such a laser.

[1] Vladan Vuletic, Nature 484 (2013)

Danksagung

Als Erstes will ich meinen Eltern für die immer motivierende Unterstützung über all die Jahre danken. Sowohl in der Schul- als auch Studienzeit halfen sie mir sowohl finanziell als auch emotional immer wieder weiter.

Bei meinem Betreuer Prof. Helmut Ritsch bedanke ich mich für die Möglichkeit an einem interessanten und wirklich aktuellen Thema zu arbeiten, dafür dass er immer ein offene Tür für Fragen und Diskussionen hatte und für die Chance die ganze Bandbreite des wissenschaftlichen Arbeitens zu erfahren.

Für die ganzen Hilfestellungen, die interessanten Debatten und für ein ausgesprochen angenehmes Arbeitsklima bedanke ich mich bei der gesamten Arbeitsgruppe. Besonders erwähnen will ich hier Laurin Ostermann, Sebastian Krämer, Wolfgang Niedenzu, Dominik Winterauer, Stefan Ostermann und, zwar nicht direkt aus unserer Arbeitsgruppe, Michael Schuler.

Weiters wäre diese Arbeit auch nicht zustande gekommen ohne meine wirklich guten und treuen Freunden, die mich stets motivierten und mich auch bei längeren Durststrecken niemals den Glauben an mein Studium bzw. an die Masterarbeit verlieren ließen, vor allem Matthias Suitner, Thomas Rabl, Michael Langer und Wolfgang Dummer.

Selbstverständlich darf ich nicht auf meine Schwestern, ihre Partner und meine Nichten vergessen, die immer für mich da waren, und regelmäßig für abwechslungsreiche, ablenkende und unterstützende Momente sorgten.

In der Hoffnung, dass ich nicht allzu viele vergessen habe, sage ich noch mal allen Genannten und nicht Genannten ein herzliches "Vergelt's Gott".

Contents

1 Motivation **1**

2 Introduction **4**

2.1 System Dynamics 4

2.1.1 Schrödinger picture 4

2.1.2 Heisenberg picture 5

2.1.3 Interaction picture 6

2.1.4 Master equation 8

2.2 Dipole-dipole-interaction and Superradiance 12

3 Laser **20**

3.1 Einstein rate-equation 20

3.1.1 Spontaneous emission 20

3.1.2 Absorption 21

3.1.3 Stimulated emission 21

3.1.4 Einstein relation 22

3.1.5 Determination of the Einstein coefficients by a quantum mechanical wave function description 23

3.2 Properties of a Laser 23

3.2.1 Pumping 24

3.2.2 Laser-cavity 24

3.2.3 Active medium 25

3.2.4 Laser linewidth and line shape 26

3.3 Quantum mechanical description of a laser 27

3.3.1 Single atom laser 27

3.3.2 Many particle laser with dipole-dipole interaction – superradiant laser 31

4 Superradiant laser dynamics with confined ensembles **35**
4.1 Emission spectrum of a superradiant laser 35
4.2 General properties of superradiant lasing 36
4.3 The superradiant lattice laser 37
4.3.1 A square lattice of four atoms 38
4.3.2 A linear chain of three atoms 38
4.3.3 Comparison of different geometric configurations 39
4.4 Laser stability and frequency shifts for different atomic distances . . . 40
4.4.1 Laser linewidth and frequency shift 40
4.4.2 Laser sensitivity to cavity length fluctuations 43

5 Conclusions and outlook **48**

Chapter 1

Motivation

The invention of the Laser has allowed many important innovations in modern sciences. For the different capabilities, different properties are most signification, e.g. a high intensity, a small bandwidth or a short pulse duration. In this thesis we are concerned with a possible candidate for an ultra frequency-stable laser system. We hope, that the realization of a superradiant laser will lay the ground for a very precise atomic clock, which is very useful for a list of applications including GPS navigation.

At the moment the limit imposed abound the bandwidth is dominated by the thermal noise (vibrations of the resonator), as shown in figure 1.1 (left). In the superradiant or bad cavity regime, in principle, it is possible to decouple the atomic polarization from the cavity mode noise [1, 3], so that the bandwidth of the out put light field mostly depends on the bandwidth of the used laser transition. For the Shawolow-Townes full-width half-maximum formula for the linewidth ($\Delta\nu$,eq. 1.1) exists two different limits one for the good, $\Gamma \gg \kappa$, and for the bad cavity case, $\Gamma \ll \kappa$, i.e.,

$$\Delta\nu_{ST} = \frac{1}{4\pi}\frac{h\nu}{P_{out}}\left(\frac{2\Gamma\kappa}{2\Gamma+\kappa}\right)^2, \tag{1.1}$$

where P_{out} is the laser power of the system, Γ represents the spontaneous emission rate and κ describes the cavity loss. A conventional laser operates in the good cavity limit. In such a system it is possible to reach smaller bandwidths by increasing the photon number, e.g. by a stronger pump. For this case the linewidth is described by

$$\Delta\nu = \frac{\kappa}{4\pi M_c}, \tag{1.2}$$

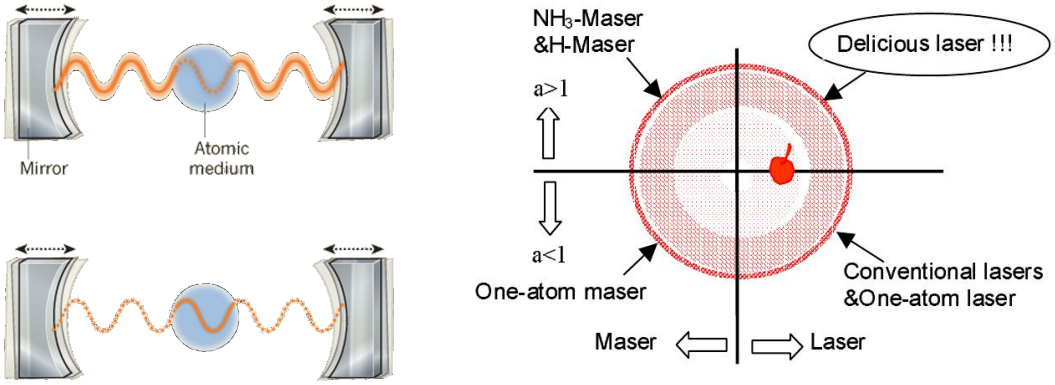

Figure 1.1: On the left-hand side, two limits are compared: the upper image represents the good cavity case with a strong intracavity light field, where the vibrations of the cavity have an impact on the laser light field. The lower schematic shows the bad cavity limit. Here almost only the stability of the atoms of the active medium is important for the bandwidth. On the right-hand side, we see the so-called maser and laser 'Birthdaycake'. (Source: [2, 3])

where M_c are the number of intracavity photons. For the superradiant (bad cavity) limit this formula simplifies to

$$\Delta\nu = \frac{\Gamma^2}{\pi\kappa M_c}. \tag{1.3}$$

If it is possible to find a system, where $\Gamma^2/\kappa < M_c$, and it can be controlled sufficient well, it becomes feasible to realize a superradiant laser with a very small bandwidth.

In fig. 1.1(right) the 'maser-laser Birthdaycake' is visualized. It has four different parts: it is divided into a laser and maser part and also into a good and bad cavity region. The upper left corner represents the bad cavity masers, e.g. the Ammonia (NH_3) maser and the one-atom Hydrogen-maser, and lower left region shows the good cavity, one atom maser. On the right-hand side we see the two laser regions with the lower corner representing conventional lasers and the upper region denoting the area, where the superradiant laser would be placed. As Chen mentioned in this figure, it should become a 'delicious laser'.

Bibliography

[1] Justin G Bohnet, Zilong Chen, Joshua M Weiner, Dominic Meiser, Murray J Holland, and James K Thompson. A steady-state superradiant laser with less than one intracavity photon. *Nature*, 484(7392):78–81, 2012.

[2] Jingbao Chen. Active Optical Clock. *Chinese Science Bulletin*, 54:348–352, 2005.

[3] Vladan Vuletic. Atomic physics: An almost lightless laser. *Nature*, 484(7392): 43–44, 2012.

Chapter 2

Introduction

In this chapter, the basic mathematical and physical principles needed to understand the formalism that describes a superradiant laser are introduced.

2.1 System Dynamics

There are different possibilities to calculate the time evolution of a quantum system. In this work we investigate a light mode coupled to a bunch of atoms (see section 3.3.2). In the following two formulations, for a closed system, which is energy conserving, and another one describing an open system, that includes an interaction with the environment, are introduced.

2.1.1 Schrödinger picture

The Schrödinger picture describes the time evolution by a constant Hamilton operators and a wave-function, which evolves in time [1, 3] according to the The Schrödinger equation

$$i\hbar\frac{\mathrm{d}}{\mathrm{d}t}\left|\psi(t)\right\rangle = H_S\left|\psi(t)\right\rangle, \tag{2.1}$$

H_S is the time-independent Hamiltonian and constitutes the energy-observable of the system, $|\psi\rangle$ is the time-dependent state vector of the system, describing the time evolution of the systems quantum state. The formal solution of eq. (2.1) is $|\psi(t)\rangle = U_S(t,0)\,|\psi(0)\rangle$, with the unitary operator $U_S(t,0) = \exp\left(-\frac{i}{\hbar}H_S t\right)$ the so-called time evolution operator in the Schrödinger picture.

To illustrate, how it is possible to calculate the time evolution of a state, let us consider an example. We choose a very simple Hamiltonian, which we will later use

to describe an electromagnetic field mode in a cavity (see section 3),

$$H_S = \sum_n \hbar\omega \left(n + \frac{1}{2}\right) |n\rangle \langle n| . \tag{2.2}$$

For this Hamiltonian the time evolution operator is

$$U(t,0) = \exp\left(-\frac{i}{\hbar} H_S t\right) = \sum_n \exp\left(-i\omega_n t\right) |n\rangle \langle n| . \tag{2.3}$$

If we choose an energy eigenstate of H as the initial state, i.e. $|\psi(0)\rangle = |m\rangle$, with $H_S |m\rangle = \hbar\omega \left(m + \frac{1}{2}\right) |m\rangle$, we obtain the time dependent state

$$|\psi(t)\rangle = \exp\left(-i\omega_m t\right) |m\rangle . \tag{2.4}$$

Here, we see that an energy eigenstate, called stationary state, remains an eigenstate in time, while only its phase is changed, which this has no physical consequence. This means that the energy of such an electromagnetic field in this state can not change. As a consequence, the systems energy is constant, what is not surprising as it is an eigenstate of the Hamiltonian and in this system no other term (interacting) exists.

2.1.2 Heisenberg picture

In this picture the quantum state $|\psi\rangle$ is constant but the operators evolve by time. An operator in the Heisenberg picture is defined as $\mathcal{O}_H(t) = e^{iHt/\hbar} \mathcal{O}_S e^{iHt/\hbar}$, $\mathcal{O}_S$ is the known operator in the Schrödinger picture. Now we calculate the time derivative of an operator in the Heisenberg picture,

$$\begin{aligned} \frac{d}{dt}\mathcal{O}_H &= \frac{iH}{\hbar} e^{iHt/\hbar} \mathcal{O}_S e^{iHt/\hbar} - e^{iHt/\hbar} \mathcal{O}_S \frac{-iH}{\hbar} e^{iHt/\hbar} \\ &= \frac{i}{\hbar} e^{iHt/\hbar} \left[H, \mathcal{O}_S\right] e^{-iHt/\hbar} = \frac{i}{\hbar} \left[H, \mathcal{O}_H(t)\right] . \end{aligned} \tag{2.5}$$

Above we have shown that the time derivation is governed by the commutator of the operator itself and the Hamiltonian.

2.1.3 Interaction picture

The interaction, or Dirac picture, is a representation fundamental for the understanding of the following kind of master equation, which will be used to describe our model of a superradiant laser. It differs from the Schrödinger picture in that the state **and** the observable are time dependent [1, 3]. This form of quantum mechanical description is useful, if it is not possible to find an analytical solution of the Schrödinger equation, or the time evolution operator, respectively. To get transform the Hamiltonian into the interaction picture, we split the system, or 'Schrödinger Hamiltonian', into two parts, $H = H_S + V$, where V is the interacting or perturbation part and H_S is the analytically exactly solvable Hamiltonian. We define the state in the interaction picture as a unitary transformation of the time dependent state we get for H_S, $|\psi_I(t)\rangle = U_S^\dagger(t,0)\,|\psi(t)\rangle$. Now, we calculate the time evolution of the state in the interaction picture to get an equation similar to the Schrödinger equation, with a new Hamiltonian for this reference frame. We call it 'the interaction Hamiltonian' $\tilde{V}(t)$. The procedure goes at follows

$$\begin{aligned}
\frac{\mathrm{d}}{\mathrm{d}t}\,|\psi_I(t)\rangle &= \left(\frac{\mathrm{d}}{\mathrm{d}t}U_S^\dagger(t,0)\right)|\psi(t)\rangle + U_S^\dagger(t,0)\frac{\mathrm{d}}{\mathrm{d}t}\,|\psi(t)\rangle \\
&= \frac{i}{\hbar}H_S U_S^\dagger(t,0)\,|\psi(t)\rangle - \frac{i}{\hbar}U_S^\dagger(t,0)H\,|\psi(t)\rangle \\
&= -\frac{i}{\hbar}U_S^\dagger(t,0)(H-H_S)\,|\psi(t)\rangle \\
&= -\frac{i}{\hbar}U_S^\dagger(t,0)(H-H_S)U_S(t,0)U_S^\dagger(t,0)\,|\psi(t)\rangle \\
&= -\frac{i}{\hbar}\tilde{V}(t)\,|\psi_I(t)\rangle\,.
\end{aligned} \tag{2.6}$$

Therefore, the transformation from the known Schrödinger Hamiltonian into the interaction Hamiltonian is

$$\tilde{V}(t) = U_S^\dagger(t,0)VU_S(t,0). \tag{2.7}$$

A laser driven two-level atom

For a better understanding of the usefulness of the interaction picture we are going to derive the dynamics of an atom, which is driven by the light field of a laser. In the following, the atom is described as a two-level system with a ground state $|g\rangle$ and an excited state $|e\rangle$. As required, we have a Hamiltonian with two parts, one

for the two-level atom, $H_A = \hbar\omega_A |e\rangle \langle e|$[1], and one for the action of the driving laser field, $H_L = \vec{E}(t) \cdot \hat{\vec{d}}$, where $\hat{\vec{d}}$ is the 3D quantum mechanical dipole operator. Now, we can rewrite this operator as:

$$\begin{aligned} \mathbf{1} \cdot \hat{\vec{d}} \cdot \mathbf{1} &= (|g\rangle \langle g| + |e\rangle \langle e|) \, \hat{\vec{d}} \, (|g\rangle \langle g| + |e\rangle \langle e|) \\ &= |g\rangle \langle g| \, \hat{\vec{d}} |g\rangle \langle g| + |g\rangle \langle g| \, \hat{\vec{d}} |e\rangle \langle e| + |e\rangle \langle e| \, \hat{\vec{d}} |g\rangle \langle g| + |e\rangle \langle e| \, \hat{\vec{d}} |e\rangle \langle e| \, . \end{aligned} \tag{2.8}$$

If we use the property that the states are either symmetric or anti-symmetric, the two terms ($\langle g| \, \vec{x} \, |g\rangle = \langle e| \, \vec{x} \, |e\rangle = 0$) in eq. (2.8) are zero, so we get

$$\hat{\vec{d}} = |g\rangle \langle g| \, \hat{\vec{d}} |e\rangle \langle e| + |e\rangle \langle e| \, \hat{\vec{d}} |g\rangle \langle g| = \hat{\vec{D}} \, |g\rangle \langle e| + \hat{\vec{D}}^* \, |e\rangle \langle g| \, , \tag{2.9}$$

with the dipole moment $\hat{\vec{D}} = \langle g| \, \hat{\vec{d}} |e\rangle$. We are now able to derive a new form of the laser interaction Hamiltonian, if we write the electric field of the laser as $\vec{E}(t) = \left(\vec{\mathcal{E}} \exp(-i\omega_0 t) + \vec{\mathcal{E}}^* \exp(i\omega_0 t) \right)$,

$$H_L = \left(\vec{\mathcal{E}} \exp(-i\omega_0 t) + \vec{\mathcal{E}}^* \exp(i\omega_0 t) \right) \cdot \left(\hat{\vec{D}} \, |g\rangle \langle e| + \hat{\vec{D}}^* \, |e\rangle \langle g| \right) . \tag{2.10}$$

For this system the atomic Hamiltonian H_A is time independent and the laser Hamiltonian H_L is the perturbation. Using eq. (2.7) and assuming that we are in the resonant case, $\omega_A = \omega_0$, the interaction picture Hamiltonian reads

$$\begin{aligned} \tilde{V}(t) =& U_S^\dagger(t,0) H_L U_S(t,0) \\ =& \vec{\mathcal{E}} \cdot \hat{\vec{D}} \exp(-2i\omega_0 t) \, |g\rangle \langle e| + \vec{\mathcal{E}} \cdot \hat{\vec{D}}^* \, |e\rangle \langle g| + \\ & \vec{\mathcal{E}}^* \cdot \hat{\vec{D}} \, |g\rangle \langle e| + \vec{\mathcal{E}}^* \cdot \hat{\vec{D}}^* \exp(2i\omega_0 t) \, |g\rangle \langle e| \end{aligned} \tag{2.11}$$

Now, we perform the rotating wave approximation by neglecting the fast rotating terms $\exp(\pm 2i\omega_0 t)$. We define a new variable, called vacuum Rabi frequency, as $\Omega \equiv \frac{2}{\hbar} \vec{\mathcal{E}} \cdot \hat{\vec{D}}^*$, and furthermore, we restrict this frequency to be a real, $\Omega = \Omega^*$. This yields the interaction Hamiltonian,

$$\tilde{V}(t) = \frac{\hbar}{2} \Omega \left(|g\rangle \langle e| + |e\rangle \langle g| \right) . \tag{2.12}$$

[1]This is equal to the later used atomic Hamiltonian, $H_A = \frac{\hbar\omega_A}{2}\sigma_z$, the difference is only that both levels have been shifted by $\frac{\hbar\omega_A}{2}$.

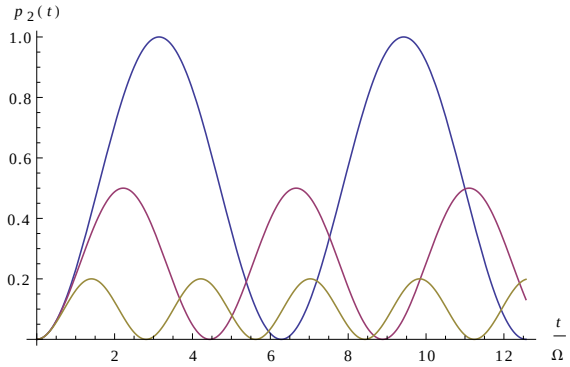

Figure 2.1: Rabi oscillation for different detunings. Blue $\Delta = 0$, red $\Delta = \Omega$ and yellow $\Delta = 2\Omega$.

By solving eq. (2.6) using this Hamiltonian with an initial state $|\psi(0)\rangle = |g\rangle$, we get a time-dependent description for the state in the interaction picture,

$$|\psi_I(t)\rangle = \cos\left(\frac{1}{2}\Omega t\right)|g\rangle - i\sin\left(\frac{1}{2}\Omega t\right)|e\rangle. \tag{2.13}$$

Now, we want to calculate the possibilities to occupy the two states, $p_g(t)$ and $p_g(t)$, so we have to compute the square of the absolute value

$$p_g(t) = \cos^2\left(\frac{\Omega t}{2}\right) = \frac{1+\cos(\Omega t)}{2} \quad \text{and} \quad p_e(t) = \sin^2\left(\frac{\Omega t}{2}\right) = \frac{1-\cos(\Omega t)}{2}. \tag{2.14}$$

This result is called Rabi cycle and is one of the most popular quantum mechanical phenomena. If we allow a detuning between the atoms and the irradiated light field, $\Delta = \omega_A - \omega_0$, so we get for upper state a possibility of $p_e(t) = \frac{\Omega^2}{\Omega'^2}\frac{1-\cos(\Omega' t)}{2}$, where $\Omega' = \sqrt{\Omega^2 + \Delta^2}$.

2.1.4 Master equation

Up until now, we have only discussed descriptions of energy conserving systems but for the more realistic description of physical phenomena, it is essential to include dissipative effects, e.g. spontaneous emission. For this, an interacting environment, called bath or reservoir, is introduced. With some assumptions and approximations, it is then possible to eliminate the bath and derive an equation for the effective dynamics of the system alone in the form of a master equation. [4, 7, 8]

To derive this time evolution it is necessary that the collective of system and

bath can be described by a quantum mechanical state vector or a density matrix[2], respectively, which has a unitary time evolution ($U(t,0) = \exp(-\frac{i}{\hbar}Ht)$), with a Hamiltonian, $H = H_S + H_B + V$. H_S is the Hamiltonian of the system, H_B describes the bath, and V is the interaction between the two constituents of the Hilbert space. The time evolution of the whole density matrix, ρ_{SB}, is analogous to the solution of the Schrödinger equation 2.1, which means

$$\rho_{SB}(t) = \exp\left[-\frac{i}{\hbar}Ht\right]\rho_{SB}(0)\exp\left[\frac{i}{\hbar}Ht\right]. \tag{2.15}$$

If we transform into the interaction picture, as introduced in section 2.1.3, we can rewrite the equation 2.15 from above as

$$\begin{aligned}\rho_{SB}(t) =& \exp\left[-\frac{i}{\hbar}(H_S+H_B)t\right]\mathcal{T}\left\{\exp\left[-\frac{i}{\hbar}\int_0^t \mathrm{d}\tau\tilde{V}(\tau)\right]\right\}\rho_{SB}(0)\\ &\times\mathcal{T}\left\{\exp\left[\frac{i}{\hbar}\int_0^t \mathrm{d}\tau\tilde{V}(\tau)\right]\right\}\exp\left[\frac{i}{\hbar}(H_S+H_B)t\right]\end{aligned} \tag{2.16}$$

with the time-ordered exponential integral

$$\begin{aligned}\mathcal{T}\left\{\exp\left[-\frac{i}{\hbar}\int_0^t \mathrm{d}\tau\tilde{V}(\tau)\right]\right\} =& 1+\sum_{n=1}^{\infty}\left(-\frac{i}{\hbar}\right)^n\int_0^t \mathrm{d}\tau_1\int_0^{\tau_1}\mathrm{d}\tau_2\cdots\\ &\times\int_0^{\tau_{n-1}}\mathrm{d}\tau_n\tilde{V}(\tau_1)\tilde{V}(\tau_2)\cdots\tilde{V}(\tau_n),\end{aligned} \tag{2.17}$$

where $t > \tau_1 > \tau_2 > \cdots$. Since we are only interested in the dynamics of the system, we are able to eliminate the bath by performing the partial trace over the baths density matrix

$$\rho(t) \equiv \rho_S(t) = \mathrm{Tr}_B\{\rho_{SB}(t)\}. \tag{2.18}$$

For this it is essential that the two subsystems are decoupled at the initial time t=0. In this way the initial state can be written as $\rho_{SB} = \rho_S(0)\otimes\rho_B(0)$. Combined with

[2] A density matrix is an operator acting on a Hilbert space, representing the possible mixed state of the system. For a pure state $|\psi\rangle$ it is the projector onto the state, $\rho = |\psi\rangle\langle\psi|$, while generally it is defined as convex combination of projectors, $\rho = \sum_i p_i |\psi_i\rangle\langle\psi_i|$, with $\sum_i p_i = 1$

eq. (2.16) and the Baker-Campell-Hausdorff formula, it results in

$$\rho(t) = \rho(0) + \sum_{n=1}^{\infty} \left(-\frac{i}{\hbar}\right)^n \mathrm{Tr}_B \left\{ \int_0^t \mathrm{d}\tau_1 \int_0^{\tau_1} \mathrm{d}\tau_2 \cdots \int_0^{\tau_{n-1}} \mathrm{d}\tau_n \times[\tilde{V}(\tau_1), [\tilde{V}(\tau_2), \cdots [\tilde{V}(\tau_n), \rho_{SB}]]] \right\}. \tag{2.19}$$

Now, we assume that $\mathrm{Tr}_B \{V(t)\rho_B\} = 0$ and use the Born approximation, which claims that the perturbation is weak and we are thus able to neglect all terms above second order. Then, the time evolution of the density matrix of the system equates to

$$\frac{\mathrm{d}}{\mathrm{d}t}\rho(t) = -\frac{1}{\hbar^2} \int_0^t d\tau \mathrm{Tr}_B \left[\tilde{V}(t), \left[\tilde{V}(t-\tau), \rho_{SB}\right]\right]. \tag{2.20}$$

Let us consider a system-bath interaction Hamiltonian of the form

$$V = \hbar \sum_{k=1}^{N} \left(c_k^\dagger d_k + c_k d_k^\dagger\right), \tag{2.21}$$

where c_k is a system operator and d_k is an operator for the reservoir and N is the number of interaction operators between the system and the environment. After a transformation into the interaction picture this looks like

$$\tilde{V}(t) = \hbar \sum_{k=1}^{N} \left(\tilde{c}_k^\dagger(t)\tilde{d}_k(t) + \tilde{c}_k(t)\tilde{d}_k^\dagger(t)\right) \tag{2.22}$$

and the operators become

$$\tilde{c}_k(t) = \exp\left(iH_S t/\hbar\right) c_k \exp\left(-iH_S t/\hbar\right), \tag{2.23a}$$

$$\tilde{d}_k(t) = \exp\left(iH_B t/\hbar\right) d_k \exp\left(-iH_B t/\hbar\right). \tag{2.23b}$$

Now, we combine eq. (2.22) and retransform of eq. (2.20) into the Schrödinger picture to get a master equation in so called Lindblad form

$$\frac{\partial \rho}{\partial t} = i\left[\rho, H_S\right] + \mathcal{L}\left[\rho\right], \tag{2.24}$$

where $\mathcal{L}[\rho]$ is the Liovillian superoperator acting on the density matrix ρ, which is

defined as

$$\begin{aligned}\mathcal{L}[\rho] = \sum_{k,l} \Big[&\left(c_k^\dagger \rho c_l - \rho c_l c_k^\dagger\right) \Gamma_{lk}^{(1)} + \left(c_k \rho c_l^\dagger - \rho c_l^\dagger c_k\right) \Gamma_{lk}^{(2)} \\ &+ \left(c_k^\dagger \rho c_l^\dagger - \rho c_l^\dagger c_k^\dagger\right) \Gamma_{lk}^{(3)} + \left(c_k \rho c_l - \rho c_l c_k\right) \Gamma_{lk}^{(4)} + h.c.\Big] .\end{aligned} \tag{2.25}$$

The different Γs are rates, which are related by two-time averages of the reservoir operators

$$\Gamma^{(1)}_{lk}(t) = \int_0^t \mathrm{d}\tau \exp\left(i\Omega_l\tau\right)\mathrm{Tr}_B\left(\tilde{d}^\dagger_l(t-\tau)\tilde{d}_k(t)\rho_B(0)\right), \tag{2.26a}$$

$$\Gamma^{(2)}_{lk}(t) = \int_0^t \mathrm{d}\tau \exp\left(i\Omega_l\tau\right)\mathrm{Tr}_B\left(\tilde{d}_l(t-\tau)\tilde{d}^\dagger_k(t)\rho_B(0)\right), \tag{2.26b}$$

$$\Gamma^{(3)}_{lk}(t) = \int_0^t \mathrm{d}\tau \exp\left(i\Omega_l\tau\right)\mathrm{Tr}_B\left(\tilde{d}_l(t-\tau)\tilde{d}_k(t)\rho_B(0)\right), \tag{2.26c}$$

$$\Gamma^{(4)}_{lk}(t) = \int_0^t \mathrm{d}\tau \exp\left(i\Omega_l\tau\right)\mathrm{Tr}_B\left(\tilde{d}^\dagger_l(t-\tau)\tilde{d}^\dagger_k(t)\rho_B(0)\right). \tag{2.26d}$$

The next step is to assume that the bath has a very short correlation time compared to the timescale of the system. For this it is essential that the bath has an infinite number of degrees of freedom, and a large bandwidth, so that the bath has no memory. This is called Markov approximation and it is possible to raise the upper integration limit to infinity.

2.2 Dipole-dipole-interaction and Superradiance

Let us present a second approach towards a master equation. In this section we derive a quantum Langevin equation for N equal two-level systems, which are coupled to a quantized field mode [5, 6, 2] and then transform this into the master equation for the system. The Hamiltonian has three parts, one for the atoms, H_a, one for the electric field, H_f and one for the interaction between the field and the atoms, H_{int}

$$H = H_a + H_f + H_{int}, \tag{2.27}$$

where

$$H_a = \sum_{i=1}^{N} \frac{\hbar\omega_a}{2}\sigma_z^i, \tag{2.28a}$$

$$H_f = \sum_{\lambda=1,2}\int d^3\vec{k}\ \hbar\omega b^\dagger_{\lambda\vec{k}} b_{\lambda\vec{k}}, \tag{2.28b}$$

$$H_{int} = \sum_{i=1}^{N}\left(\vec{\mu}_{eg}\sigma_i^+ + \vec{\mu}_{ge}\sigma_i^-\right)\vec{E}(\vec{x_i}). \tag{2.28c}$$

Here ω_a is the transition frequency of the atom, $b^\dagger_{\lambda\vec{k}}$ and $b_{\lambda\vec{k}}$ are the creation and annihilation operators for the light mode with the frequency ω and wave vector $\vec{k}$. σ_i^+ and σ_i^- are the rising and lowering operator of the i-th atom and $\vec{E}(\vec{x}) = \vec{E}^{(+)}(\vec{x}) + \vec{E}^{(-)}(\vec{x})$ is the electric field, which is described by

$$\vec{E}^{(+)}(\vec{x}) = \sum_\lambda \int d^3k \mathcal{E}_k \vec{\epsilon}_{\lambda\vec{k}} b_{\lambda\vec{k}} e^{i\vec{k}\vec{x}}, \text{ with } \mathcal{E}_k := i\sqrt{\frac{\hbar\omega}{2\epsilon_0(2\pi)^3}}, \tag{2.29}$$

where $\epsilon_{\lambda\vec{k}}$ is the relative permittivity and $\vec{E}^{(-)}$ is defined as the complex conjugated of $\vec{E}^{(+)}$.

The positions of the atoms are assumed as fixed in these Hamiltonians, such that we neglect any motion of the atoms. In practice that could be realized by a well engineered optical lattice, where one atom sits in every lattice site as in a so-called Mott state. Further, it is important that the distance between two atoms is larger than the Bohr radius, otherwise it is very likely that other effects, e.g. forming of molecules, came into play. Now, we calculate the Heissenberg-Langevin equation for all b_k-operators under the assumption that $\vec{\mu} \equiv \vec{\mu}_{eg} = \vec{\mu}_{ge}$, which corresponds to the quantized Maxwell equation

$$\dot{b}_{\lambda\vec{k}}(t) = \frac{i}{\hbar}\left[H(t), b_{\lambda\vec{k}}(t)\right] = -i\omega b_{\lambda\vec{k}}(t) + \frac{i}{\hbar}\mathcal{E}_k^* \vec{\mu}\cdot\vec{\epsilon}_{\lambda\vec{k}} \left(\sum_{\alpha=1}^N e^{-i\vec{k}\vec{x}\alpha} s_\alpha(t)\right), \tag{2.30}$$

where $s_\alpha \equiv \sigma_\alpha^+ + \sigma_\alpha^-$. With the solution of eq. (2.30), we get an expression for the dipole interaction

$$\begin{aligned}\vec{\mu}\cdot\vec{E}^{(+)}(\vec{x},t) =& \vec{\mu}\cdot\vec{E}^{(+)}_{in}(\vec{x},t) + \\ & \frac{i}{\hbar}\sum_\lambda \int d^3k |\mathcal{E}_k \vec{\mu}\cdot\vec{\epsilon}_{\lambda\vec{k}}|^2 \times \\ & \times \int_{t_0}^t dt' e^{-i\omega(t-t')} \left(\sum_{\alpha=1}^N e^{-i\vec{k}(\vec{x}-\vec{x}_\alpha)} s_\alpha(t')\right)\end{aligned} \tag{2.31}$$

In this formula the integral represents the retarded Green function. Now, we are

able to calculate the equation of motion for any atomic system operator $c(t)$,

$$\begin{aligned}\dot{c}(t) = \quad & i\left[\sum_{\alpha=1}^{N}\frac{\hbar\omega_a}{2}\sigma_z(t), c(t)\right] \\ & -\frac{i}{\hbar}\sum_{\alpha=1}^{N}\left[s_\alpha(t), c(t)\right]\vec{\mu}\cdot\vec{E}^{(+)}(\vec{x}_\alpha, t) - \frac{i}{\hbar}\sum_{\alpha=1}^{N}\vec{\mu}\cdot\vec{E}^{(-)}(\vec{x}_\alpha, t)\left[s_\alpha(t), c(t)\right].\end{aligned} \tag{2.32}$$

We replace $\vec{\mu}\cdot\vec{E}^{(\pm)}$ with this expression from eq. (2.31) so that the second line of eq. (2.32) becomes

$$\begin{aligned}& -\frac{i}{\hbar}\sum_{\alpha=1}^{N}\left[s_\alpha(t), c(t)\right]\vec{\mu}\cdot\vec{E}^{(+)}(\vec{x}_\alpha, t) - \frac{i}{\hbar}\sum_{\alpha=1}^{N}\vec{\mu}\cdot\vec{E}^{(-)}(\vec{x}_\alpha, t)\left[s_\alpha(t), c(t)\right] \\ & + \frac{1}{\hbar^2}\sum_\lambda\int d^3k|\mathcal{E}_k\vec{\mu}\cdot\vec{\epsilon}_{\lambda\vec{k}}|^2\int_{t_0}^{t}dt' e^{-i\omega(t-t')}\left\{\sum_{\alpha,\beta}e^{i\vec{k}\vec{x}_{\alpha\beta}}[s_\alpha(t), a(t)]s_\beta(t')\right\} \\ & - \frac{1}{\hbar^2}\sum_\lambda\int d^3k|\mathcal{E}_k\vec{\mu}\cdot\vec{\epsilon}_{\lambda\vec{k}}|^2\int_{t_0}^{t}dt' e^{i\omega(t-t')}\left\{\sum_{\alpha,\beta}e^{-i\vec{k}\vec{x}_{\alpha\beta}}s_\beta(t')[s_\alpha(t), a(t)]\right\} =: (*),\end{aligned} \tag{2.33}$$

with $\vec{x}_{\alpha\beta} = \vec{x}_\alpha - \vec{x}_\beta$. We use $\sum_\lambda|\vec{\mu}\cdot\vec{\epsilon}_{\lambda\vec{k}}| = \vec{\mu}^2 - (\hat{\vec{k}}\cdot\vec{\mu})^2$ with the unit wave vector $\hat{\vec{k}} = \vec{k}/k$ and get

$$\begin{aligned}(*) = & -\frac{i}{\hbar}\sum_{\alpha=1}^{N}\left[s_\alpha(t), c(t)\right]\vec{\mu}\cdot\vec{E}^{(+)}(\vec{x}_\alpha, t) - \frac{i}{\hbar}\sum_{\alpha=1}^{N}\vec{\mu}\cdot\vec{E}^{(-)}(\vec{x}_\alpha, t)\left[s_\alpha(t), c(t)\right] \\ & + \frac{\vec{\mu}^2}{2\hbar\epsilon_0}\frac{1}{(2\pi c)^3}\sum_{\alpha,\beta}\int d\Omega_{\vec{k}}\left[1-(\vec{k}\cdot\vec{\mu})^2\right]\int_{t_0}^{t}dt'\int_0^\infty\omega^3 d\omega\; e^{-i\omega(t-t'-\vec{k}\vec{x_{\alpha\beta}}/c)}\left[s_\alpha(t), c(t)\right]s_\beta(t') \\ & - \frac{\vec{\mu}^2}{2\hbar\epsilon_0}\frac{1}{(2\pi c)^3}\sum_{\alpha,\beta}\int d\Omega_{\vec{k}}\left[1-(\vec{k}\cdot\vec{\mu})^2\right]\int_{t_0}^{t}dt'\int_0^\infty\omega^3 d\omega\; e^{i\omega(t-t'-\vec{k}\vec{x_{\alpha\beta}}/c)}s_\beta(t')\left[s_\alpha(t), c(t)\right].\end{aligned} \tag{2.34}$$

Moreover, we replace $s_\beta(t')$ with $\sigma_\beta^+(t)e^{i\omega_a(t-t')} + \sigma_\beta^-(t)e^{-i\omega_a(t-t')}$, calculate the retarded Green function[3] and integrate over the solid angle and frequency. Finally, we perform

[3] If we perform the positive limit for $\epsilon(t\to 0^+)$ we end up with

$$\begin{aligned}\int_{t_0\to-\infty}^{t}dt' e^{-i(\omega-i\epsilon\pm\omega_{eg})(t-t')} &= \frac{1}{i(\omega-i\epsilon\pm\omega_{eg})} \equiv -i\mathcal{P}\frac{1}{\omega\pm\omega_{eg}} + \pi\delta(\omega-\omega_{eg}) \\ \int_{t_0\to-\infty}^{t}dt' e^{i(\omega-i\epsilon\pm\omega_{eg})(t-t')} &= \frac{1}{-i(\omega-i\epsilon\pm\omega_{eg})} \equiv +i\mathcal{P}\frac{1}{\omega\pm\omega_{eg}} + \pi\delta(\omega-\omega_{eg})\end{aligned}$$

the rotating wave approximation and for for eq. (2.33) we get

$$
\begin{aligned}
(*) = &- \frac{i}{\hbar}\sum_{\alpha=1}^{N}\left[s_\alpha(t), c(t)\right]\vec{\mu}\cdot\vec{E}^{(+)}(\vec{x}_\alpha, t) - \frac{i}{\hbar}\sum_{\alpha=1}^{N}\vec{\mu}\cdot\vec{E}^{(-)}(\vec{x}_\alpha, t)\left[s_\alpha(t), c(t)\right] \\
&+ \sum_{\alpha,\beta}[s_\alpha(t), a(t)]\frac{\Gamma}{k_a^3}\int_0^\infty \frac{dk}{2\pi}k^3 F(kr_{\alpha\beta}) \\
&\left\{\left(-i\mathcal{P}\frac{1}{k+k_a} + \pi\delta(k+k_a)\right)\sigma_\beta^+(t) + \left(-i\mathcal{P}\frac{1}{k-k_a} + \pi\delta(k-k_a)\right)\sigma_\beta^-(t)\right\} \\
&- \sum_{\alpha,\beta}\frac{\Gamma}{k_a^3}\int_0^\infty \frac{dk}{2\pi}k^3 F(kr_{\alpha\beta})\times \\
&\times\left\{\sigma_\beta^+(t)\left(+i\mathcal{P}\frac{1}{k+k_a} + \pi\delta(k+k_a)\right) + \sigma_\beta^-(t)\left(+i\mathcal{P}\frac{1}{k-k_a} + \pi\delta(k-k_a)\right)\right\}\times \\
&\times [s_\alpha(t), a(t)].
\end{aligned}
\tag{2.35}
$$

Here, $\Gamma = \frac{k_a^3}{3\pi\hbar\epsilon_0}|\vec{\mu}|^2$ is the single atom spontaneous emission rate and

$$
\begin{aligned}
F(\xi) :=& \int \frac{d\Omega_{\vec{k}}}{4\pi}\left[1 - (\hat{\vec{k}}\cdot\hat{\vec{\mu}})^2\right]e^{ik_0 r\hat{\vec{k}}\hat{\vec{r}}_{\alpha\beta}} \\
=& \frac{\sin\xi}{\xi}\left(1 - \left(\hat{\vec{\mu}}\cdot\hat{\vec{r}}_{\alpha\beta}\right)^2\right) + \left(1 - 3\left(\hat{\vec{\mu}}\cdot\hat{\vec{r}}_{\alpha\beta}\right)^2\right)\left(\frac{\cos\xi}{\xi^2} - \frac{\sin\xi}{\xi^3}\right),
\end{aligned}
\tag{2.36}
$$

with $\xi \equiv k_0 r_{\alpha\beta}$ Now, it is possible to define collective decay rates and energy shifts introduced by the dipole-dipole interaction,

$$
\Gamma_{\alpha\beta} = \frac{3}{2}\Gamma F(kr_{\alpha\beta}), \tag{2.37}
$$

$$
\Omega_{\alpha\beta}^{\pm} := \frac{\Gamma}{k_a^3}\int_0^\infty \frac{dk}{2\pi}\frac{k^3 F(kr_{\alpha\beta})}{k \pm k_a}. \tag{2.38}
$$

With this definitions eq. (2.35) assumes a much simpler form, such that the entire

optical Bloch equation looks as follows

$$\begin{aligned}\dot{c}(t) = & \frac{i}{\hbar}\left[\sum_{\alpha=1}^{N}\left\{\hbar(\omega_a-\Omega_{\alpha\alpha}^{-})\sigma_\alpha^{+}(t)\sigma_\alpha^{-}(t)+\hbar(-\Omega_{\alpha\alpha}^{+}\sigma_\alpha^{-}(t)\sigma_\alpha^{+}(t))\right\},c(t)\right] \\ & +\frac{i}{\hbar}\left[\sum_{\alpha\neq\beta}\hbar\Omega_{\alpha\beta}\sigma_\alpha^{-}(t)\sigma_\beta^{+}(t),c(t)\right] \\ & -\frac{i}{\hbar}\sum_{\alpha=1}^{N}\left[\sigma_\alpha^{+}(t),c(t)\right]\vec{\mu}\cdot\vec{E}^{(+)}(\vec{x}_\alpha,t)-\frac{i}{\hbar}\sum_{\alpha=1}^{N}\vec{\mu}\cdot\vec{E}^{(-)}(\vec{x}_\alpha,t)\left[\sigma_\alpha^{-}(t),c(t)\right] \\ & +\frac{1}{2}\sum_{\alpha,\beta}\Gamma_{\alpha\beta}\left\{2\sigma_\alpha^{+}(t)c(t)\sigma_\alpha^{+}-\sigma_\alpha^{+}(t)\sigma_\beta^{-}(t)c(t)-c(t)\sigma_\alpha^{+}(t)\sigma_\beta^{-}(t)\right\}.\end{aligned} \tag{2.39}$$

The expression in the first braces is an "infinite" Lamb shift, which we are able to absorb into the atomic transition frequency. [9]

$$\Omega_{\alpha\beta}:=-\Omega_{\alpha\beta}^{+}-\Omega_{\alpha\beta}^{-}=-\frac{3\Gamma}{(k_{eg}r_{\alpha\beta})^3}\mathcal{P}\int_{-\infty}^{+\infty}\frac{d\xi}{4\pi}\frac{\xi^3F_{\alpha\beta}(\xi)}{\xi-k_{eg}r_{\alpha\beta}}=\frac{3\Gamma}{4}G_{\alpha\beta}(k_{eg}r_{\alpha\beta}). \tag{2.40}$$

Furthermore, in equation (2.40) we recover the expression for the coherent term or the so-called energy shift caused by the dipole-dipole interaction

$$G_{\alpha\beta}(\xi)=-\left(1-\cos^2\theta\right)\frac{\cos\xi}{\xi}+\left(1-3\cos^2\theta\right)\left(\frac{\xi}{\xi^2}+\frac{\cos\xi}{\xi^3}\right). \tag{2.41}$$

Finally, the master equation for N atoms with dipole-dipole interaction can be written as

$$\dot{\rho}(t)=-\frac{i}{\hbar}\left[\sum_{\alpha=1}^{N}\tilde{H}_{sys},\rho(t)\right]+\frac{1}{2}\sum_{\alpha,\beta=1}^{N}\Gamma_{\alpha\beta}\left(2\sigma_\alpha^{-}\rho(t)\sigma_\beta^{+}-\sigma_\alpha^{+}\sigma_\beta^{-}\rho(t)-\rho(t)\sigma_\alpha^{+}\sigma_\beta^{-}\right), \tag{2.42}$$

with

$$\begin{aligned}H_{sys}=&\sum_{\alpha=1}^{N}\left\{\hbar\omega_a\sigma_\alpha^{+}\sigma_\alpha^{-}-\vec{\mu}\cdot\vec{E}^{(+)}(\vec{x}_\alpha,t)\sigma_\alpha^{+}(t)-\vec{\mu}\cdot\vec{E}^{(-)}(\vec{x}_\alpha,t)\sigma_\alpha^{-}(t)\right\}+ \\ &\sum_{\alpha\neq\beta=1}^{N}h\Omega_{\alpha\beta}\sigma_\alpha^{-}\sigma_\beta^{+}\end{aligned} \tag{2.43}$$

Let us consider two atoms at first. In figure 2.2 we see how the dipole interaction

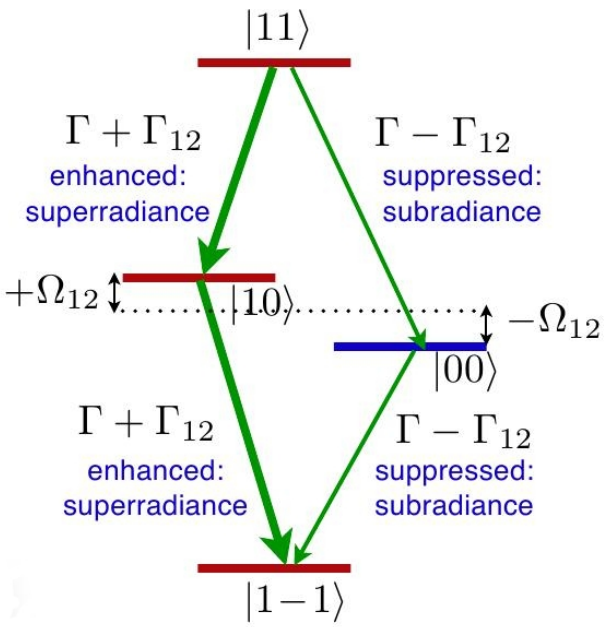

Figure 2.2: A symbolic illustration of the collective properties of two two-level atoms coupled via a the dipole-dipole interaction. (Source: [9])

acts on the energy levels of two two-level atoms. As calculated, we have two different terms, a coherent one $\sum_{\alpha,\beta}^{N} \Omega_{\alpha\beta}\sigma_{\alpha}^{+}\sigma_{\beta}^{-}$, which causes a frequency shift of the atom excitation frequency and a dissipative term (see second part of eq. (2.42)), which causes a alteration of the decay rate. If we switch to the eigenbasis of H_{sys} and introduce triplet and a singlet state, we are able to represent the energy levels as seen in figure 2.2, where the triplet consists of the doubly excited state $|ee\rangle$, the ground state $|gg\rangle$ and the symmetric superposition of the states with one excited atom $\frac{1}{\sqrt{2}}(|eg\rangle + |ge\rangle)$ and the singlet state is the antisymmetric superposition $\frac{1}{\sqrt{2}}(|eg\rangle - |ge\rangle)$ similar to a dark state. To get a better understanding of the collective decay $\Gamma_{\alpha\beta}$ and the energy shift $\Omega_{\alpha,\beta}$, in figure 2.3 the related functions $F_{\alpha\beta}(\xi)$ and $G_{\alpha\beta}(\xi)$ are plotted for two different configurations. At first, where the dipole's orientation is perpendicular to the relative position vector of the two atoms and secondly where the two vectors are parallel.

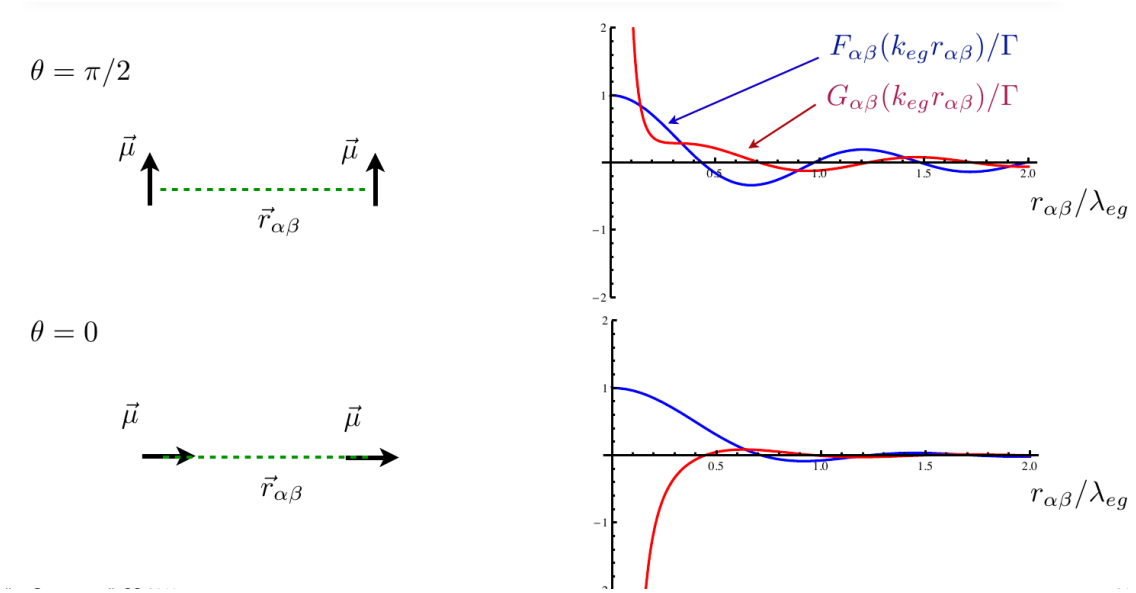

Figure 2.3: The collective decay $F_{\alpha\beta}/\Gamma$ of dipole-dipole atoms and the energy shift $G_{\alpha\beta}/\Gamma$ for two-different geometrical alignments. (Source: [9])

Bibliography

[1] A. Beige. Introductory Quantum Optics , 2007.

[2] R. H. Dicke. Coherence in Spontaneous Radiation Processes. *Phys. Rev.*, 93: 99–110, 1954. doi: 10.1103/PhysRev.93.99. URL `http://link.aps.org/doi/10.1103/PhysRev.93.99`.

[3] C. W. Gardiner and P. Zoller. *Quantum Noise*. Springer-Verlag, second enlarged edition, 2000.

[4] A. Kossakowski. On quantum statistical mechanics of non-Hamiltonian systems. *Reports on Mathematical Physics*, 3(4):247–274, 1972.

[5] R. H. Lehmberg. Radiation from an N-Atom System. I. General Formalism. *Phys. Rev. A*, 2:883–888, Sep 1970. doi: 10.1103/PhysRevA.2.883. URL `http://link.aps.org/doi/10.1103/PhysRevA.2.883`.

[6] R. H. Lehmberg. Radiation from an N-Atom System. II. Spontaneous Emission from a Pair of Atoms. *Phys. Rev. A*, 2:889–896, Sep 1970. doi: 10.1103/PhysRevA.2.889. URL `http://link.aps.org/doi/10.1103/PhysRevA.2.889`.

[7] R. R. Puri. *Mathematical Methods of Quantum Optics*. Springer Series in Optical Science. Springer-Verlag, 2001.

[8] D. F. Walls and G. J. Milburn. *Quantum Optics*. Springer-Verlag, 2nd edition, 2008.

[9] P. Zoller. Vorlesung Quantenoptik, SS 2011.

Chapter 3

Laser

3.1 Einstein rate-equation

Now, we want to discuss the different microscopic processes of how an atom, approximated by a two-level system, interacts with an electromagnetic field [1, 4, 13]. In the following we describe the progresses acting on an ensemble of equal atoms.

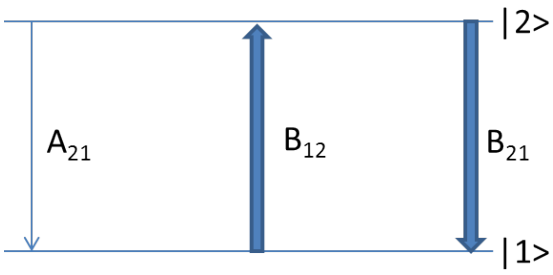

Figure 3.1: Schematic picture of the possible absorption and emission processes of a two-level atom.

3.1.1 Spontaneous emission

First, we have to consider that some of the two-level atoms are excited, which means they are in the upper energetic level $|2\rangle$. Excited atoms are able to emit a photon with a certain rate A_{21} and are transferred to the ground state $|1\rangle$ subsequently. The emitted photon possesses the transition energy, which is the energetic difference of the two levels, $h\nu = E_2 - E_1$. A_{21} is called the Einstein coefficient of spontaneous

emission. We describe the population change of the excited level N_2 induced by spontaneous emission by

$$\mathrm{d}N_2 = -A_{21}N_2 dt \rightarrow N_2(t) = N_2(0)e^{-A_{21}t} \equiv N_2(0)e^{-t/\tau_{sp}}, \tag{3.1}$$

where $N_2(0)$ is the number of excited atoms at the beginning of the observation. We are able to define $\tau_{sp} = \frac{1}{A_{21}}$ as the average lifetime of an excited atom, also known as the spontaneous lifetime. Further, from the uncertainty principle we can borrow a relation between the average lifetime and the uncertainty in transition energy, $\Delta E \cdot \Delta t \geqslant \frac{\hbar}{2}$. If we have a very long-lived state[1] the uncertainty of the frequency of the emitted photon is very small. This effect is important for the in superradiant laser, because we aim for a small as possible bandwidth.

3.1.2 Absorption

If atoms are in the ground state, $|1\rangle$, and an electromagnetic field is present, it is possible that one of them absorbs a photon and is excited to the upper level $|2\rangle$. This population change of the ground state can also be described by a differential rate equation

$$\mathrm{d}N_1 = -B_{12}u(\nu)N_1 dt. \tag{3.2}$$

Analogy to equation (3.1), N_1 is the number of two-level systems in the ground state, B_{12} is the Einstein coefficient of absorption and $u(\nu)$ is the spectral energy density of the surrounding electromagnetic field. From eq. (3.2) we see that an energy field around the atoms is necessary to excite them in the first place, and that the excitation possibility directly depends on the intensity of the field.

3.1.3 Stimulated emission

The stimulated or induced emission is the counterpart of the absorption process, because both describe an interaction between a photon and an atom, the stimulated emission with an excited atom and the absorption with an atom in the ground state, respectively. This means that with a certain probability a photon, with an energy similar to the transition energy, can stimulate an excited atom to emit a photon with the same properties, i.e. the same phase, frequency and polarization. Here, we also

[1] For a long-lived state the statistical dispersion of the moment, when the excited atom decays, is larger as for a fast decaying one.

define a rate B_{21}, which is called the Einstein coefficient of stimulated emission.

$$\mathrm{d}N_2 = -B_{21}u(\nu)N_2 dt \tag{3.3}$$

Contrary to the spontaneous emission, the absorption and stimulated emission are coherent processes, which means that they depend on the radiation field. Coherent processes do not affect the existing phase relationship of the present electromagnetic field.

3.1.4 Einstein relation

Now, we combine these three different dynamical processes for two-level atoms to obtain a better understanding and calculate a relation between these rates in order to find a population equilibrium. The system of differential equations for the populations of the upper and lower state reads

$$\frac{\mathrm{d}}{\mathrm{d}t}N_1 = -N_1 B_{12}u + N_2 B_{21}u + N_2 A_{21}, \tag{3.4a}$$

$$\frac{\mathrm{d}}{\mathrm{d}t}N_2 = +N_1 B_{12}u - N_2 B_{21}u - N_2 A_{21}. \tag{3.4b}$$

These two equations are conected, in such a way that the number of atoms is constant for every time step, i.e., $N_0 = N_1 + N_2 \overset{!}{=} \text{const.}$. To calculate the steady state for this system of differential equations we set its time derivative to zero. This leads to a linear equation for the spectral energy density

$$u(\nu) = \frac{A_{21}/B_{21}}{(B_{21}/B_{12}) \cdot (N_1/N_2) - 1}. \tag{3.5}$$

In a typical setup we consider a black body radiation, so $u(\nu)$ underlies Planckian distribution [12]

$$u(\nu, T)\mathrm{d}\nu = \frac{8\pi\nu^3}{c^3}\left[e^{h\nu/k_B T} - 1\right]^{-1}\mathrm{d}\nu, \tag{3.6}$$

and the population of the states is described by the Boltzmann statistics

$$\frac{N_2}{N_1} = \frac{g_2}{g_1}\, e^{-(E_2 - E_1)/k_B T}, \tag{3.7}$$

where g_1 and g_2 are the degrees of degeneracy of the states $|1\rangle$ and $|2\rangle$. From this the proportions between the absorption and stimulated emission Einstein coefficients

and between the spontaneous and stimulated emission Einstein coefficients are

$$B_{12} = \frac{g_2}{g_1} B_{21}, \tag{3.8}$$

$$A_{21} = \frac{8\pi\nu^3}{c^3} B_{21} = h\nu Z(\nu) B_{21}. \tag{3.9}$$

$Z(\nu)$ represents the density of the states.

These two relations are universal and do not depend on atomic species or the chosen two levels.

3.1.5 Determination of the Einstein coefficients by a quantum mechanical wave function description

For a quantum mechanical description of the stimulated emission, it is absolutely essential to characterize both levels by a wave function ψ_i. With this it is possible to write down the dipole matrix element for an electric dipole transition,

$$\vec{\mu}_{21} = -\int \psi_2^* \, e \cdot \vec{r} \, \psi_1 \mathrm{d}V. \tag{3.10}$$

If we consider a constant spectral energy density, $\rho(\nu) \equiv \rho$, eq. (3.8) change to [**?**]

$$\begin{aligned} B_{21} &= \frac{2\pi^2 |\vec{\mu}_{21}|^2}{3\epsilon_0 h^2} = B_{12}, \\ A_{21} &= \frac{8\pi\nu^3}{c^3} B_{21} = \frac{16\pi^3\nu^3 |\vec{\mu}_{21}|^2}{3\epsilon_0 h c^3}. \end{aligned} \tag{3.11}$$

Now, these equations for the rates depend on the quantum mechanical dipole matrix element $\vec{\mu}_{21}$ as defined above.

3.2 Properties of a Laser

The first proposal to build a laser (**l**ight **a**mplification by **s**timulated **e**mission of **r**adiation) was put forward by C. H. Townes and A. L. Shawlow [14], although they called it an optical maser in the beginning.

This section will briefly introduce the concept of the functionality of a laser, illustrate, which components are indispensable for its operation and highlight some features of the different elements of this tool.

3.2.1 Pumping

'Pumping' refers to the process, which provides the system with energy by exciting the atoms or molecules of the active, or gain medium, which is placed in between two high quality mirrors, i.e., is a cavity). In order to archive lasing it is necessary that enough energy is put into the system to create an inversion of the population on the laser transition. In terms of experimental setups there are many different possibilities to realize this and also in theory several options to describe this effect exist.

Historically, the first laser, the Ruby laser by T. Maiman [6], was pumped by a Xenon flash tube. Beside this first successful implementation, lasers have been pumped by chemical reactions, gas discharges, electric fields etc.

For the mathematical characterization of pumping, there are two important decisions one has to make. Firstly, one has to decide, if the pumping process is transverse or longitudinal to the cavity axis and secondly weather it is a coherent or an incoherent one. As mentioned above, a process which depends on the present light field is called coherent. If we talk about coherent pumping, it is a part of the Hamiltonian, whereas an incoherent one is represented as one of the Liouvillian terms. For our model of a superradiant laser, we always use a transverse incoherent pumping.

3.2.2 Laser-cavity

In a common laser an optical-cavity is necessary to define its mode. As mentioned in chapter 1, for the conventional type of a laser, the linewidth of the cavity is much smaller than the bandwidth of the active medium (see fig. 3.2). Cavities are like a Fabry-Perot interferometer, one can calculate the so-called free spectral range[2] for the cavity

$$\Delta\nu = \frac{c}{2L}, \tag{3.12}$$

with $L = \int_0^x n(s)ds$ the optical, and x the geometric distance between the two mirrors, where $n(s)$ represents the refraction index of the medium in between.

Usually, more than one cavity mode fits into the gain bandwidth, but most of the time only the one with the largest gain survives in the laser light field. We assume a linear cavity in the following model.

[2]The FSR is the frequency difference between two neighbouring cavity modes.

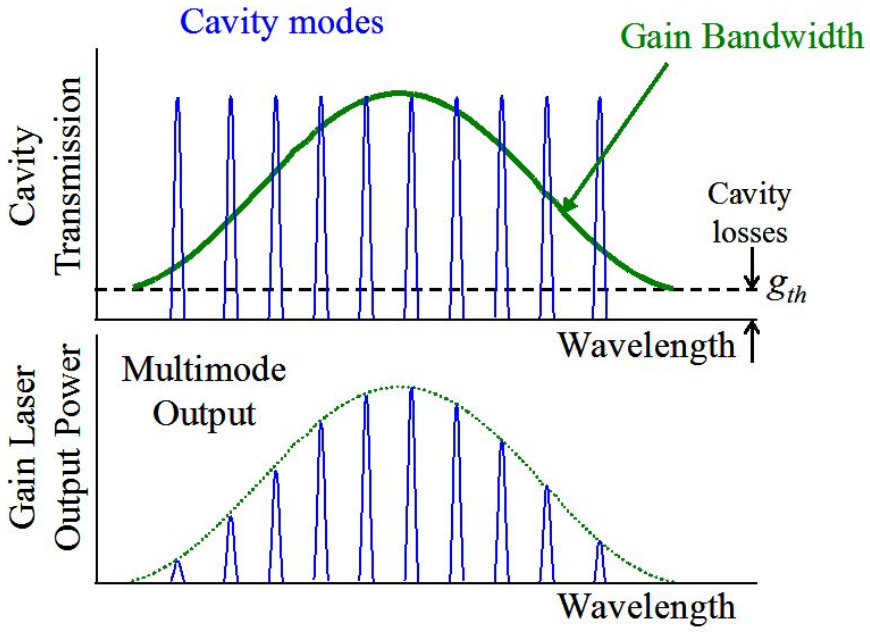

Figure 3.2: A comparison of the active medium bandwidth and the bandwidth of the cavity modes. Usually, only the mode with the highest gain survives. (Source: [11])

3.2.3 Active medium

The active medium, also called gain medium, is the main ingredient of a laser. Its characteristics are primarily determined by the active medium. Prominent examples are the color, i.e. the frequency, of the laser light. To build a working laser, a three- or four-level system is required to even enable inversion of the state occupation, as discussed below. Real atomic systems are (of course) more complicated. Fig. 3.2.3 shows two possible transition sequences realizing a superradiant laser, one with Barium (Ba) and a second one for Strontium (Sr).

In the following theoretical treatment we will describe the atoms of the active medium as two-level systems to minimize the Hilbert space allowing faster calculations. Although, it is not possible to archive inversion with a two-level system, as the occupation of the states underlies the Boltzmann statistics, which means we can at best reach an equilibrium between the two populations by an infinitely strong pumping. However, we can introduce an artificial effective pumping rate, R, which compensates the fact that we neglect the third and fourth level. The biggest difference between the setup of a superradiant laser and a regular one is the choice of the laser transition. In a conventional laser an as high as possible photon number is required.

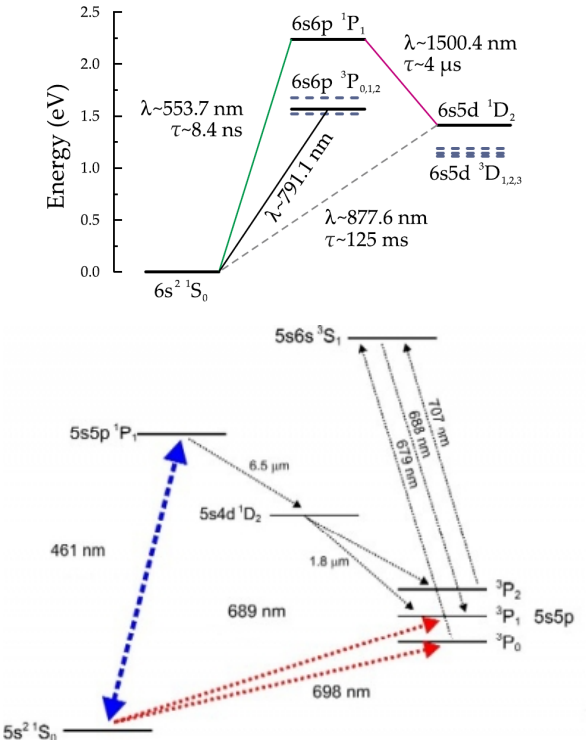

Figure 3.3: The energy levels of neutral Barium (Ba) (left). A possible transition series for the superradiant laser, where the laser transition is between $^1D_2$ and $^1S_0$, and is pumped through $^1P_1$. For Strontium (Sr) (right) it would be an option to pump from $^1Sr_0$ to $^1P_1$ and decay to the upper laser states $^3P_0$ via $^1D_2$. (Source: [9, 8])

This is why usually very fast decaying laser transitions are preferred, while in our case we strive to using a relatively long-lived upper laser state. In this way the emitted light should have a smaller bandwidth.

3.2.4 Laser linewidth and line shape

Besides the power, a very narrow linewidth is one of the most important qualities of a laser. The Scully-Lamb theory [15] described the two-level laser in terms of second quantization for the first time. With this approach the first models of how it would be possible to calculate the linewidth and also the spectral profile of a laser could be derived [16].

In the following to calculate the spectral distribution of the light field inside the

cavity, $S(\omega, t)$, we make use of the Wiener-Khinchin theorem [7],

$$S(\omega,\, t) = \int e^{-i\omega\tau} \left\langle a^\dagger(t+\tau)a(t)\right\rangle \,\mathrm{d}\tau, \tag{3.13}$$

where the relative spectrum is described by the Fourier transformation of the two time field correlation function. Numerically, this is calculated by at first determining the steady state ρ_S, which can be calculated as the kernel of the master equation, i.e. solving $\frac{\partial\rho}{\partial t} = i\left[\rho, H\right] + \mathcal{L}\left[\rho\right] = 0$. Now, the annihilation operator a is applied and we let this state evolve. After a time τ has elapsed, we apply the creation operator $a^\dagger$ and Fourier-transform the trace of this aggregate.

For almost coherent light, as it should be the case for a laser, the spectrum follows a Lorentzian distribution. Later on, in the numerical simulations (see chapter 4) we fit a Lorentzian to the normalized spectrum. Then, the width of the fitted curve describes the bandwidth of the intra-cavity light field.

3.3 Quantum mechanical description of a laser

Until now, we have presented very general properties of lasers. In this section the quantum mechanical model of the system under consideration in this work is introduced, first for a single pumped atom inside a cavity, then we expand this to a many-particle model with dipole-dipole interaction between the individual atoms.

3.3.1 Single atom laser

Here, we consider a pumped two-level atom inside a high-Q optical resonator with one cavity mode. Further, we employ a transverse incoherent pump which allows us to use the atom as an active medium. In addition two dissipative processes, namely the cavity loss and spontaneous emission of the atom, are present. Upon Born, rotating wave and Markov approximation we end up with a standard Lindblad type master equation,

$$\frac{\partial\rho}{\partial t} = i\left[\rho, H\right] + \mathcal{L}\left[\rho\right], \tag{3.14}$$

with the Hamiltonian H and the Liouvillian $\mathcal{L}$. The Hamiltonian describes the atom, the cavity and also the interaction between them,

$$H = \frac{\omega_0}{2}\,\sigma^z + \omega_c\, a^\dagger a + H_{\mathrm{int}}, \tag{3.15}$$

where σ_z is the occupation of the states separated by transition energy ω_0 and the operators $a^\dagger$ and a correspond to the creation and annihilation of a photon with the frequency ω_c in the cavity mode, while

$$H_{\text{int}} = g\left(a\sigma^+ + a^\dagger\sigma^-\right), \tag{3.16}$$

where σ^+ and σ^- are the raising and lowering operators for the atomic dipole. This represents the so-called Jaynes Cummings interaction between the atom and the cavity mode with a coupling constant g. The spontaneous emission is described by the Liouvillian

$$\mathcal{L}_{\text{sp}}[\rho] = \frac{\Gamma}{2}\left(2\sigma^-\rho\sigma^+ - \sigma^+\sigma^-\rho - \rho\sigma^+\sigma^-\right), \tag{3.17}$$

with the spontaneous emission rate Γ. The incoherent transverse pumping is given by

$$\mathcal{L}_{\text{pump}}[\rho] = \frac{R}{2}\left(2\sigma^+\rho\sigma^- - \sigma^-\sigma^+\rho - \rho\sigma^-\sigma^+\right), \tag{3.18}$$

where R is to the pumping rate. Finally, the cavity loss with a loss rate of κ is accounted by

$$\mathcal{L}_{\text{cav}}[\rho] = \kappa\left(2a\rho a^\dagger - a^\dagger a\rho - \rho a^\dagger a\right). \tag{3.19}$$

Derivation of the photon number in a single atom laser

In order to gain a principle insight and check the validity of our simulation we attempt to treat the master equation analytically. Thus, we derive the so-called Ehrenfest equations [3] for our system, which equates to computing the equation of motion for the expectation value of the light field lowering operator $\langle a\rangle$, which turns out to depend on another different other expectation values, like $\langle\sigma^-\rangle$, which in turn

depends on further expectation values, like $\langle \sigma_z a \rangle$, and so on.

$$\frac{\mathrm{d}}{\mathrm{d}t}\langle a\rangle = -\kappa\langle a\rangle - ig\langle\sigma^-\rangle \tag{3.20a}$$

$$\frac{\mathrm{d}}{\mathrm{d}t}\langle a^\dagger a\rangle = -2\kappa\langle a^\dagger a\rangle - 2g\ \mathrm{Im}\langle\sigma^+ a\rangle \tag{3.20b}$$

$$\frac{\mathrm{d}}{\mathrm{d}t}\langle\sigma^-\rangle = \left(i\Delta - \frac{R}{2} - \frac{\Gamma}{2}\right)\langle\sigma^-\rangle - ig\langle\sigma_z a\rangle \tag{3.20c}$$

$$\frac{\mathrm{d}}{\mathrm{d}t}\langle\sigma_z\rangle = -(R+\Gamma)\langle\sigma_z\rangle + (R-\Gamma) + 4g\ \mathrm{Im}\langle\sigma^+ a\rangle \tag{3.20d}$$

$$\frac{\mathrm{d}}{\mathrm{d}t}\langle\sigma^+ a\rangle = \left(-i\Delta - \frac{R}{2} - \frac{\Gamma}{2} - \kappa\right)\langle\sigma^+ a\rangle - ig\langle\sigma_z a^\dagger a\rangle - ig\frac{1+\langle\sigma_z\rangle}{2} \tag{3.20e}$$

$$\begin{aligned}\frac{\mathrm{d}}{\mathrm{d}t}\langle\sigma_z a\rangle = &-(R+\Gamma+\kappa)\langle\sigma_z a\rangle + (R-\Gamma)\langle a\rangle - 2ig\langle\sigma^+ a^2\rangle + \\ &+ig\langle\sigma^-\rangle + 2ig\sigma^- a^\dagger a\end{aligned} \tag{3.20f}$$

$$\begin{aligned}\frac{\mathrm{d}}{\mathrm{d}t}\langle\sigma^+ a^2\rangle = &\left(-i\Delta - \frac{R}{2} - \frac{\Gamma}{2} - 2\kappa\right)\langle\sigma^+ a^2\rangle - \\ &-ig\langle\sigma_z a^\dagger a^2\rangle - ig\langle a\rangle - ig\langle\sigma_z a\rangle\end{aligned} \tag{3.20g}$$

$$\begin{aligned}\frac{\mathrm{d}}{\mathrm{d}t}\langle\sigma^- a^\dagger a\rangle = &\left(i\Delta - \frac{R}{2} - \frac{\Gamma}{2} - 2\kappa\right)\langle\sigma^- a^\dagger a\rangle + \\ &+ig\langle\sigma_z a^\dagger a^2\rangle - i\frac{g}{2}\langle\sigma_z a\rangle + i\frac{g}{2}\langle a\rangle\end{aligned} \tag{3.20h}$$

$$\begin{aligned}\frac{d}{dt}\langle\sigma_z a^\dagger a\rangle = &-(R+\Gamma+2\kappa)\langle\sigma_z a^\dagger a\rangle + (R-\Gamma)\langle a^\dagger a\rangle + \\ &+4g\ \mathrm{Im}\langle\sigma^+ a^\dagger a^2\rangle + 2g\ \mathrm{Im}\langle\sigma^+ a\rangle\end{aligned} \tag{3.20i}$$

To find a closed system of differential equations, we have to truncate this series by neglecting the higher order correlations $\langle\sigma_z a^\dagger a^2\rangle$ and $\langle\sigma^+ a^\dagger a^2\rangle$. This is justify by assuming a very small photon number and therefor a double annihilation is very unlikely.

If we also assume the photon number $\langle a^\dagger a\rangle \equiv \langle n\rangle$ and the inversion of the atoms

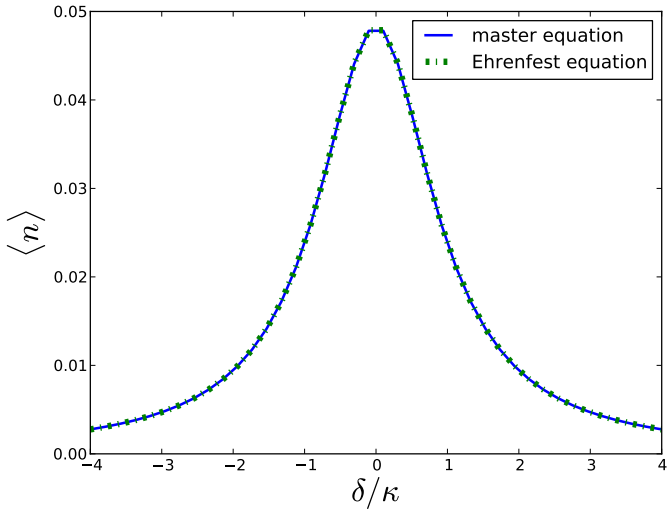

Figure 3.4: Comparison of the expectation value of the photon number computed by the Ehrenfest theorem (green doted line) with the one obtained by solving the master equation (blue solid line).

$\langle \sigma_z \rangle$ to be very small, it is possible to obtain a reduced set of differential equations.

$$\frac{\mathrm{d}}{\mathrm{d}t}\langle a^\dagger a\rangle = -2\kappa\langle a^\dagger a\rangle - 2g\ \mathrm{Im}\langle \sigma^+ a\rangle \tag{3.21a}$$

$$\frac{\mathrm{d}}{\mathrm{d}t}\langle \sigma_z\rangle = -(R+\Gamma)\langle \sigma_z\rangle + (R-\Gamma) + 4g\ \mathrm{Im}\langle \sigma^+ a\rangle \tag{3.21b}$$

$$\frac{\mathrm{d}}{\mathrm{d}t}\langle \sigma^+ a\rangle = \left(-i\Delta - \frac{R}{2} - \frac{\Gamma}{2} - \kappa\right)\langle \sigma^+ a\rangle - ig\langle \sigma_z a^\dagger a\rangle - ig\frac{1+\langle \sigma_z\rangle}{2} \tag{3.21c}$$

$$\frac{d}{dt}\langle \sigma_z a^\dagger a\rangle = -(R+\Gamma+2\kappa)\langle \sigma_z a^\dagger a\rangle + (R-\Gamma)\langle a^\dagger a\rangle + 2g\ \mathrm{Im}\langle \sigma^+ a\rangle \tag{3.21d}$$

With this set we are able to derive the expectation value of the photon number $\langle a^\dagger a\rangle$ for the steady state depending on the system variables.

$$\langle a^\dagger a\rangle = \frac{4g^2 R\gamma}{4\kappa(R+\Gamma)(\Delta^2+\gamma^2) - 2g^2\left([R-2\kappa]^2 - [\Gamma+2\kappa] - 4\kappa^2\right)} \tag{3.22}$$

Fig. 3.4 compares the photon number depending on the detuning, between the cavity mode and the atomic transition energy, δ computed by the Ehrenfest theorem to the one results by solving the master equation. As expected, both lines agree very well.

3.3.2 Many particle laser with dipole-dipole interaction – superradiant laser

In this section the model of a single atom laser is extended to many atoms and an interaction between them. To realize that, we consider N identical two-level atoms held in a regularly spaced configuration, e.g. in a far detuned optical trap, each of them symmetrically coupled to a single mode of a high Q optical resonator. A possible setup is depicted in fig. 3.5. Due to the inherent exposure of the atoms to the vacuum bath the ensemble is affected by coherent dipole-dipole energy exchange processes and also by collective spontaneous emission [5]. Similarly to the previous section we assume a transverse incoherent pump, which is equal for all atoms, and cavity loss. The time-dependence of the N-atom density matrix is again described explicitly by a Lindblad type master equation with almost the same Hamiltonian as before, except that we have to include a sum over the atoms and account for the fact that we get an extra energy exchange term from the dipole-dipole interaction amongst them,

$$H = \frac{\omega_0}{2} \sum_i \sigma_i^z + \sum_{i \neq j} \Omega_{ij}\, \sigma_i^+ \sigma_j^- + \omega_c\, a^\dagger a + H_{\text{int}}, \tag{3.23}$$

where σ_i^+ and σ_i^- are the raising and lowering operators for the atomic dipole of the i-th atom with the transition energy ω_0, and Ω_{ij} denotes the resonant dipole-dipole energy transfer between the atoms i and j. H_{int} is again the Jaynes-Cummings term, featuring the same coupling constant g for each atom. This approximation is justified in the situation where the atomic ensemble is aligned transverse to the propagation direction of the cavity mode or its dimensions are much smaller than the length of the resonator. The **collective** atomic damping is accounted for by the Liouvillian

$$\mathcal{L}_{\text{cd}}[\rho] = \frac{1}{2} \sum_{i,j} \Gamma_{ij} \left(2\sigma_i^- \rho \sigma_j^+ - \sigma_i^+ \sigma_j^- \rho - \rho \sigma_i^+ \sigma_j^- \right) \tag{3.24}$$

with generalized spontaneous emission rates Γ_{ij} arising from the coupling of the atomic transition dipoles through the vacuum field [2]. The incoherent transverse broadband pumping, which in our model acts on each atom in the same way, leads to an extra sum over the atoms of the active medium only, i.e.,

$$\mathcal{L}_{\text{pump}}[\rho] = \frac{R}{2} \sum_i \left(2\sigma_i^+ \rho \sigma_i^- - \sigma_i^- \sigma_i^+ \rho - \rho \sigma_i^- \sigma_i^+ \right) \tag{3.25}$$

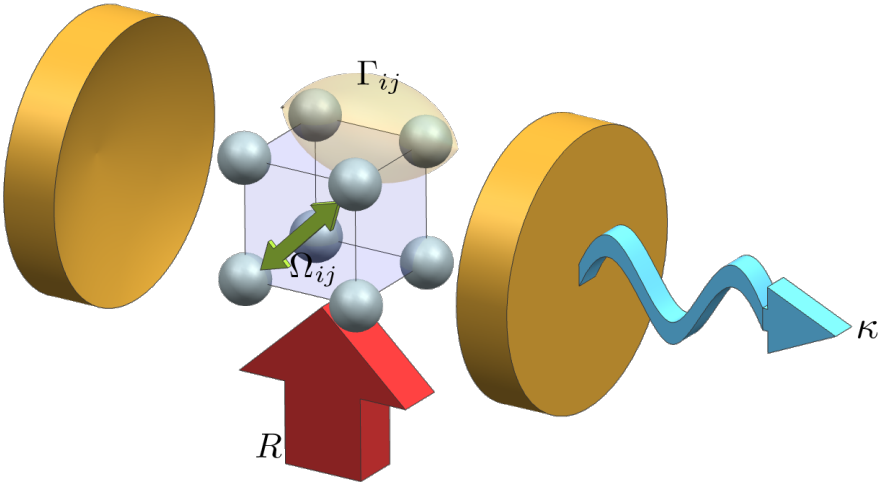

Figure 3.5: Schematics of a lattice laser setup. A transversely pumped (pumping rate R) finite atomic ensemble with dipole-dipole couplings Ω_{ij} and collective spontaneous emission Γ_{ij} inside an optical resonator with a loss rate of κ.

Note, that the collective coupling and decay matrices $[\Omega_{ij}]$ and $[\Gamma_{ij}]$ possess non-diagonal elements, which have to be calculated as a function of the system's geometry [10] (more details in sec. 2.2). In some cases, due to the finite correlation length of vacuum fluctuations, these nondiagonal parts can be safely neglected. As a reminder of section 2.2 the two expressions look like

$$\Gamma_{ij} = \frac{3\Gamma}{2} F\left(k_0 r_{ij}\right) \qquad \Omega_{ij} = \frac{3\Gamma}{4} G\left(k_0 r_{ij}\right) \tag{3.26}$$

with Γ the single atom linewidth, $k_0 = \omega_0/c = 2\pi/\lambda_0$

Bibliography

[1] A. Einstein and P. Ehrenfest. Zur Quantentheorie des Strahlungsgleichgewichts. *Zeitschrift für Physik*, 19(1):301–306, 1923. ISSN 0044-3328. doi: 10.1007/BF01327565. URL http://dx.doi.org/10.1007/BF01327565.

[2] Z. Ficek, R. Tanaś, and S. Kielich. Quantum beats and superradiant effects in the spontaneous emission from two nonidentical atoms. *Physica A: Statistical Mechanics and its Applications*, 146(3):452–482, 1987.

[3] K. Henschel, J. Majer, J. Schmiedmayer, and H. Ritsch. Cavity QED with an ultracold ensemble on a chip: Prospects for strong magnetic coupling at finite temperatures. *Physical Review A*, 82(3):033810, 2010.

[4] F.K. Kneubühl and M.W. Sigrist. *Laser*. Teubner Studienbcher Physik. Vieweg+Teubner Verlag, 2008. ISBN 9783835101456. URL http://books.google.at/books?id=o-wVcscyv1EC.

[5] R. H. Lehmberg. Radiation from an N-Atom System. I. General Formalism. *Phys. Rev. A*, 2:883–888, Sep 1970. doi: 10.1103/PhysRevA.2.883. URL http://link.aps.org/doi/10.1103/PhysRevA.2.883.

[6] T. H. Maiman. Stimulated Optical Radiation in Ruby. *Nature*, 187(4736): 493–494, 1960. doi: 10.1038/187493a0. 10.1038/187493a0.

[7] P. Meystre and M. Sargent. *Elements of Quantum Optics*. Springer-Verlag, 1990.

[8] NPL. Strontium Lattice Clock. http://www.npl.co.uk/science-technology/time-frequency/research/optical-frequency-standards/strontium-lattice-clock, May 2014.

[9] C. Ohae, A. Fukumi, S. Kuma, Y. Miyamoto, K. Nakajima, I. Nakano, H. Nanjo, N. Sasao, S. Uetake, T. Wakabayashi, et al. Production of Ba Metastable State via Superradiance. *Journal of the Physical Society of Japan*, 83(4), 2014.

[10] L. Ostermann, H. Zoubi, and H. Ritsch. Cascaded collective decay in regular arrays of cold trapped atoms. *Opt. Express*, 20, 2012. ISSN 29634-29645.

[11] R. A. Perez-Herrera and M. Lopez-Amo. *Multi-Wavelength Fiber Lasers*. intechopen, 2013.

[12] Max Planck. Ueber das Gesetz der Energieverteilung im Normalspectrum. *Annalen der Physik*, 309(3):553–563, 1901. ISSN 1521-3889. doi: 10.1002/andp.19013090310. URL http://dx.doi.org/10.1002/andp.19013090310.

[13] K.F. Renk. *Basics of Laser Physics: For Students of Science and Engineering*. Graduate Texts in Physics. Springer, 2012. ISBN 9783642235658. URL http://books.google.at/books?id=dpVDTLPySTQC.

[14] A. L. Schawlow and C. H. Townes. Infrared and Optical Masers. *Phys. Rev.*, 112:1940–1949, Dec 1958. doi: 10.1103/PhysRev.112.1940. URL http://link.aps.org/doi/10.1103/PhysRev.112.1940.

[15] M. O. Scully and W. E. Lamb. Quantum Theory of an Optical Maser. I. General Theory. *Phys. Rev.*, 159:208–226, Jul 1967. doi: 10.1103/PhysRev.159.208. URL http://link.aps.org/doi/10.1103/PhysRev.159.208.

[16] M. O. Scully and W. E. Lamb. Quantum Theory of an Optical Maser. II. Spectral Profile. *Phys. Rev.*, 166:246–249, Feb 1968. doi: 10.1103/PhysRev.166.246. URL http://link.aps.org/doi/10.1103/PhysRev.166.246.

Chapter 4

Superradiant laser dynamics with confined ensembles

Most results presented in this chapter are published in [7].

4.1 Emission spectrum of a superradiant laser

The phase of the output field of a laser underlies random fluctuations induced by various noise processes, e.g. spontaneous emission. Generally, its Fourier-transform reassemble a Lorentzian. Therefore, in the following numerical simulation we fit a Lorentzian to the numerically calculated spectrum. We suppose that the width of the the fitted curve represents the bandwidth of the system under consideration. This assumption is valid only in the region above the laser threshold, as we can see in fig. 4.1. Below the threshold often times multiple peaks are visible. Those can be categorized into simulations with little interaction and no detuning between the atoms and the cavity, where the spectra are symmetrically arranged around the cavity frequency, and heavily interacting or detuned cases, where the spectrum is dominated by one of the two peaks. For double peak spectra a Lorentzian fit to determine the width of the curve is not a suitable instrument. Yet, this area is fairly uninteresting for the quality of the laser anyway, so we do not improve the fitting process.

A little below the laser limit the shape of the spectrum changes to a single peak, which above threshold becomes narrow, which will be discussed later on.

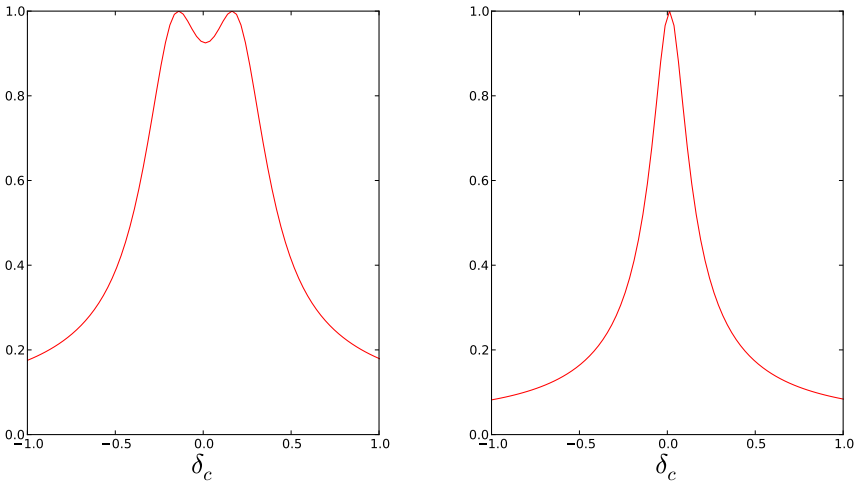

Figure 4.1: Examples for the spectrum of the superradiant laser, one below (left) and above (right) the laser threshold.

4.2 General properties of superradiant lasing

First, let us exhibit some general features of the dynamics of a laser with all atoms coupled equally to the cavity mode in the two idealized limiting cases of (a) fully collective and (b) individual independent spontaneous decay. Mathematically, this is implemented simply by setting (a) $\Gamma_{ij} = \Gamma$ for the collective case as discussed in [5] and (b) $\Gamma_{ij} = \Gamma\delta_{ij}$ for independent decay as studied in [8]. Surprisingly, the fully collective case is much easier to deal with numerically as the total collective spin magnitude is conserved and the Hilbert space for N atoms is restricted to the $N + 1$ states of a spin-1/2-system. The effective pumping of the atoms can also be described as an independent or collective phenomenon, which results in analogous expressions to those describing the respective decay processes (see 3.24). Here we refrain from including dipole-dipole induced excitonic shifts of the energy levels.

This assumption can be justified for a completely homogeneous atomic density [4] but has to be reconsidered for concrete finite size implementations or optical lattice. We will explicitly account for this in the finite lattice geometries discussed below.

Fig. 4.2 shows the mean photon number as a function of the pump strength R and the single atom decay rate Γ for the three cases of collective pump and collective decay, individual pump and collective decay and independent pump and independent decay for $N = 4$. We see that the maximum photon number is not so different for the three cases and appears at small spontaneous decay rates. For fully collective

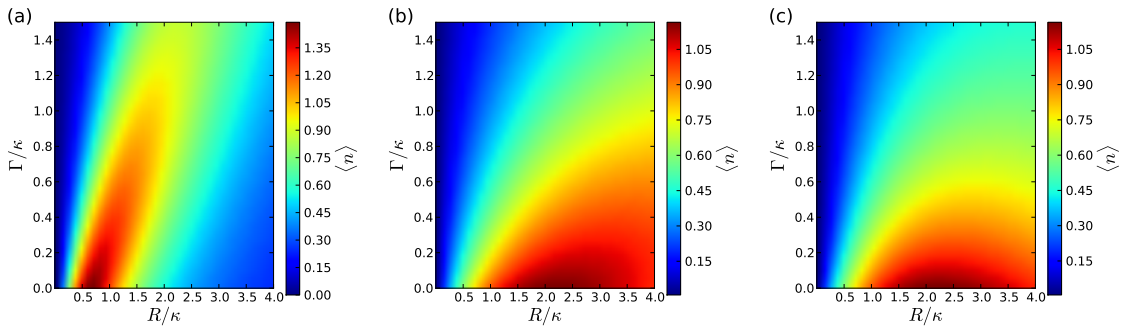

Figure 4.2: Stationary photon number as a function of the pump strength R and the spontaneous decay rate Γ for collectively pumped and collectively decaying atoms (a), individually pumped but collectively decaying atoms (b) and individually pumped and individually decaying atoms (c).

pump and collective spontaneous decay, fig. 4.2(a), superradiant emission into free space limits the optimal operation regime to a lower pump intensity, though.

Now, it is of course most interesting to look at the frequency stability or linewidth of this laser. As seen in fig. 4.3 the output intensity spectrum exhibits a nonlinear growth with the atom number (green line), as expected, until it saturates (red line). Remarkably, however, the linewidth does not narrow with the photon or atom number, but is even increased by superradiant spontaneous emission. Thus, the optimal case seems to be collective emission into the lasing mode without superradiant spontaneous decay. We will investigate this in more detail in the following sections.

4.3 The superradiant lattice laser

Above we have seen that collective decay and collective pump strongly change the laser dynamics and its properties. Besides modified decay rates governed by eq. (3.24) in any finite size geometry dipole-dipole interaction as given by eq. (3.23) has to be taken into account as well. To study the basic physical effects, in this section we will investigate three different regular geometric arrangements for the laser active atoms. We compare a linear chain, where we go beyond the single excitation and nearest-neighbor coupling limits discussed in [11], to an equilateral triangle and a square configuration. Let us point out, that for two atoms, e.g. [3], the particular relative arrangement is irrelevant, and therefore the system can be handled analytically.

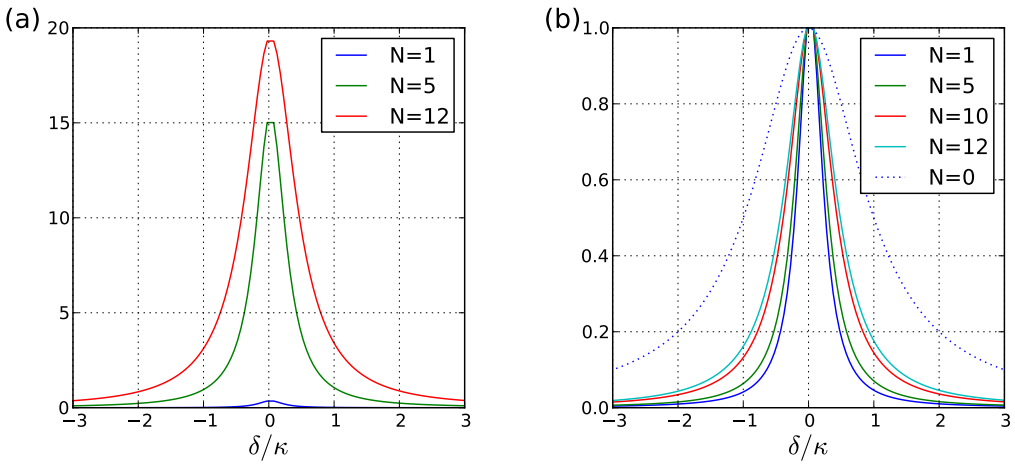

Figure 4.3: Output spectrum of a fully collective laser with different atom numbers N for $\Gamma = \kappa/20$ and $R = \kappa/5$ compared to the empty cavity linewidth ($N = 0$), absolute (left) and normalized (right).

4.3.1 A square lattice of four atoms

We first show the photon number, the inversion of the active medium atoms and the $g^{(2)}(0)$ correlation function for a fixed cavity loss κ while tuning the pumping rate R and the individual atom decay rate Γ for a four atom laser in a square lattice. The chosen lattice constant is half of the magic wavelength for Strontium, $\lambda_{magic}/(2\lambda_0) \approx 0.58$ (see [2, 10]). For the photon number shown in fig. 4.4(a) the maximum appears at a pumping ratio of $R/\kappa = 2.2$, which is equal to the result from above for individual pumping and collective decay as depicted in fig. 4.2(b).

In fig. 4.4(b) the expectation value of the σ_z-operator is illustrated, where the black line represents the crossover to population inversion. On the right-hand side of the line the atomic population is inverted, corresponding to the lasing case. Fig. 4.4(c) presents the $g^2(0)$ function, where the white line highlights a value of $g^2(0) = 1$, indicating a perfectly coherent light field. The area where $g^2(0) < 1$ could be referred to as an anti-bunching regime.

4.3.2 A linear chain of three atoms

As an addition to the square lattice, here, the result for a further kind of lattice is shown. In fig. 4.6 we present the same quantities as above for a tripartite chain. Furthermore, in fig. 4.5 we see the energy scheme of a chain of three atoms, where the fastest loss or superradiant decay channel is to go from $|e\rangle = |eee\rangle$ over the

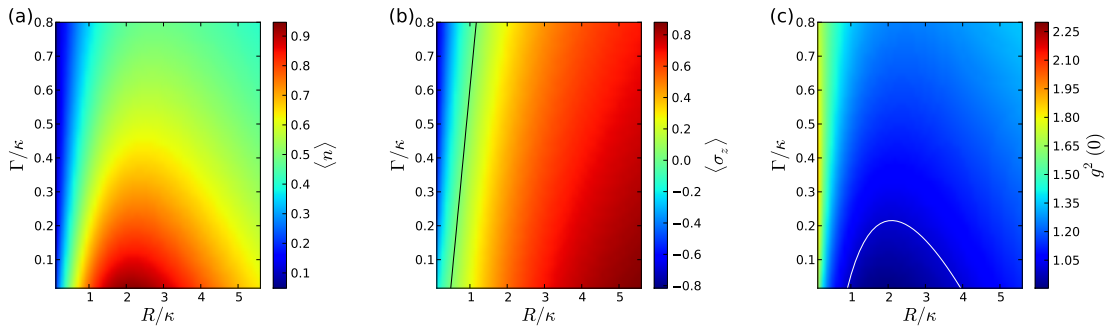

Figure 4.4: Stationary operation of a four atom laser on a square lattice. (a) photon number, (b) atomic inversion, where the black line indicates equal population of the excited and the ground state, (c) $g^2(0)$ function, with the white line at $g^{(2)}(0) = 1$ representing a coherent state

states $|2_z\rangle = |eeg\rangle + |ege\rangle + |gee\rangle$, which is the symmetric superposition of all doubly excited states and $|1_z\rangle = |egg\rangle + |geg\rangle + |gge\rangle$, the symmetric singly excited state, to $|g\rangle = |ggg\rangle$, as discussed in[9].

4.3.3 Comparison of different geometric configurations

Let us study the influence of the geometric arrangement of the particles for different numbers of atoms and compare the results for the square and triangle discussed above to a three and four atom chain. In order to obtain a substantial effect despite our small atom numbers, we choose a smaller lattice constant of $d = \lambda_0/10$ and a fixed atomic decay rate of $\Gamma/\kappa = 0.2$.

In fig. 4.7 we show, that for the average values the atom number is more important than the particular geometric arrangement. Interestingly for four atoms one can even reach sub Poissonian photon statistics.

Naturally, the results depend on the average distance of the atoms, which is symmetric shown in the following set of pictures in fig. 4.8 for a square of different lattice constants d with a fixed spontaneous emission rate of $\Gamma/\kappa = 0.2$. As one might have expected, fig. 4.8 demonstrates a much more pronounced effect when varying the distance as opposed to changing the geometry.

Overall, despite fairly strong interactions of the atoms at small distances, the laser seems to be very robust against such pairwise perturbations, which appear to average out quite well once the oscillation threshold is surpassed. The differences increase with pump strength where, on average, more particles are excited.

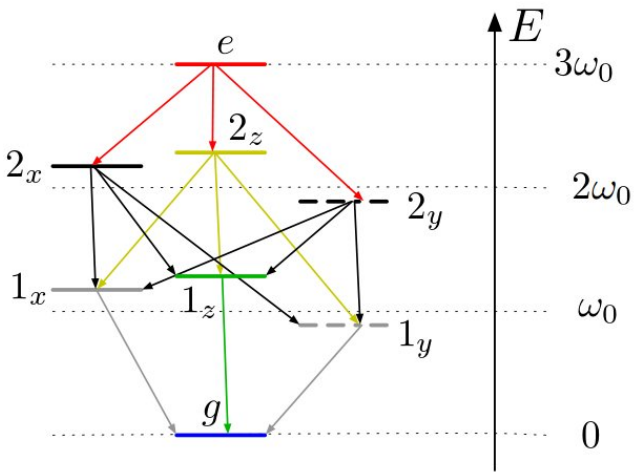

Figure 4.5: Decay scheme of three atoms in a chain configuration, but for our chosen Hamiltonian the energy scale has to go from $-\frac{3\omega_0}{2}$ to $\frac{3\omega_0}{2}$ (Source:[9])

4.4 Laser stability and frequency shifts for different atomic distances

Of course, the most sought after quality of a superradiant laser is its superb frequency stability and accuracy. In the first section we have seen that collective spontaneous decay can broaden the laser line. As dipole-dipole interactions shift the atomic energy levels, this might as well change the laser line position, which we will study for a lattice laser in more detail in the following.

4.4.1 Laser linewidth and frequency shift

As is well known, the spectrum of a laser in the bad cavity limit deviates from the idealized Shawlow-Townes result, but the center of the line still approximately follows a Lorentzian [6] so that in our numerical analysis the linewidth and its center position relative to the bare atom line can be determined from a Lorentzian fit to the steady state spectrum, as described in sec. 2. Therefore, the width of the Lorentzian corresponds to the laser's linewidth while the offset in the maximum describes the energy shift, which is the energy of the light field in the cavity relative to the cavity ground frequency. Fig. 4.9 and fig. 4.10 present the fitted width γ_L and the energy shift δ for different interatomic distances and geometric configurations as a function of the pumping rate R. For these calculations we used the same

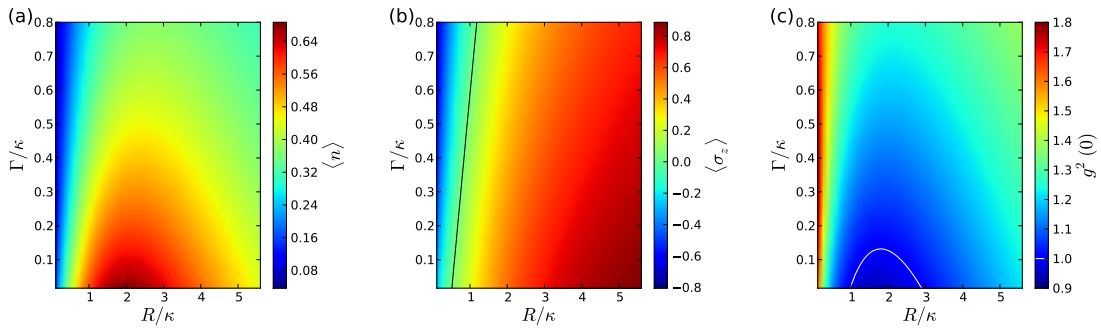

Figure 4.6: Stationary operation of a three atom laser on a chain lattice. (a) photon number, (b) atomic inversion, where the black line indicates equal population of the excited and the ground state, (c) $g^2(0)$ function, with the white line at $g^{(2)}(0) = 1$ representing a coherent state.

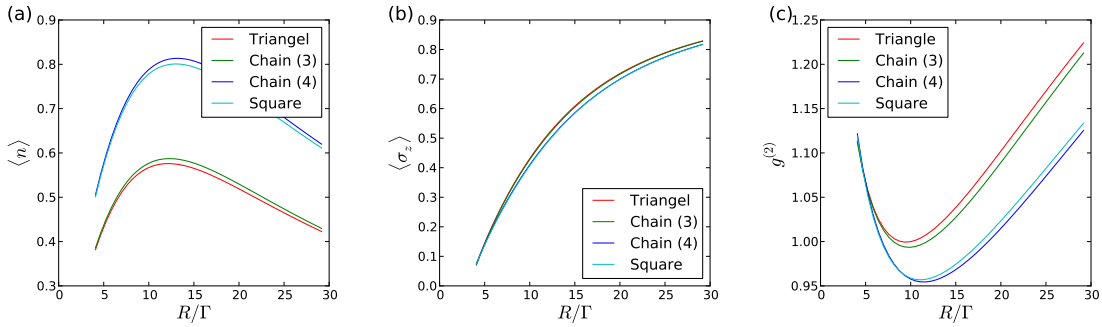

Figure 4.7: Photon number (a), atomic inversion (b) and g^2 function (c) of our laser as a function of the pump strength R for different atomic arrangements and a fixed spontaneous decay rate $\Gamma = 0.2\kappa$.

parameters as above and we do not include a detuning between the atoms and the cavity mode($\Delta = \omega_c - \omega_0 = 0$).

In fig. 4.9 we depict the linewidth and frequency shift of a laser with four atoms in a square configuration as a function of the pump strength for different interatomic distances. We observe a minimum linewidth at a moderate pump strength of $R/\kappa \approx 1.9$, which corresponds to an operation at the maximally achievable photon number, as shown in fig. 4.4.

For a stronger pump the perturbations due to collective interactions dominate, though significant effects appear for very closely positioned atoms, i.e. $d < \lambda_0/2$, only. Even with just four atoms it is possible to achieve a linewidth significantly below the resonator's linewidth. The predicted frequency shift with respect to the bare atom frequency (as depicted in fig. 4.9) remains very small for larger interatomic distances

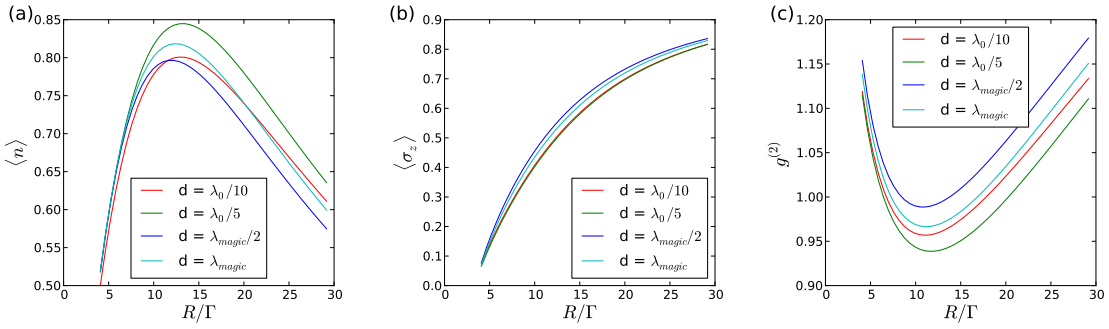

Figure 4.8: Photon number (a), atomic inversion (b) and g^2 function (c) of our laser as a function of the pump strength R for a square of different lattice constants d and a fixed spontaneous decay rate $\Gamma = 0.2\kappa$.

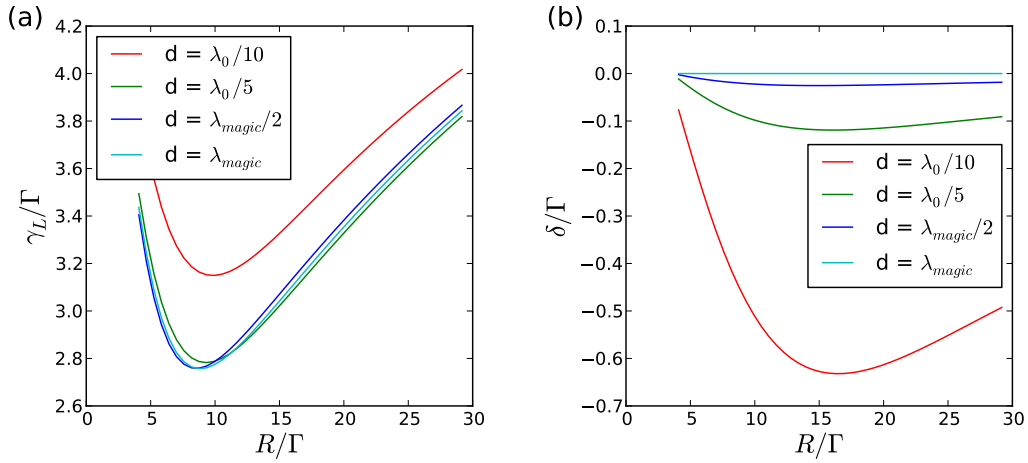

Figure 4.9: Laser linewidth (left) and frequency shift (right) for a square atom arrangement at different distances as a function of the pump strength for a fixed atomic decay rate of $\Gamma = 0.2\kappa$.

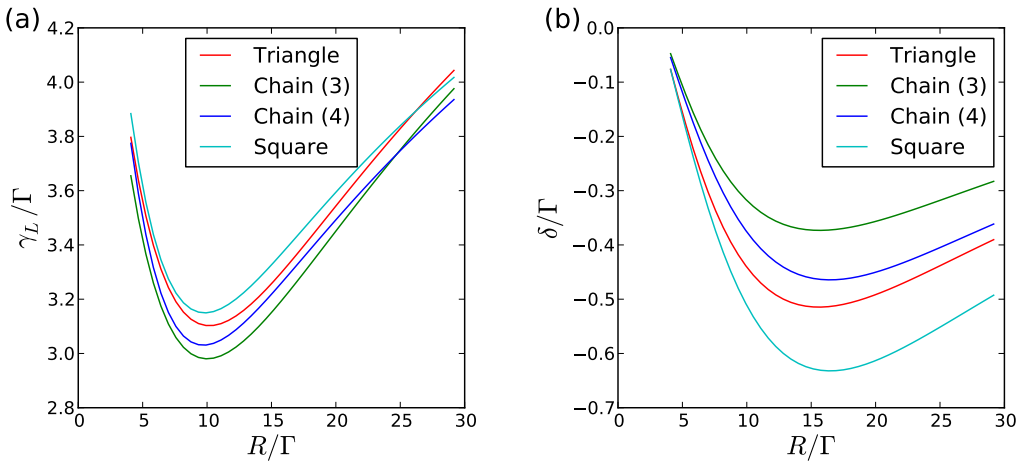

Figure 4.10: Laser linewidth (left) and frequency shift (right) for different geometric configurations and equal lattice constant ($d = \lambda_0/10$) as a function of the pump strength for a fixed atomic decay rate of $\Gamma = 0.2\kappa$.

and reaches a maximum value when the laser is operated at $R/\kappa \approx 3$, close to the maximum photon number. This could certainly be an observable phenomenon, but it is not detrimental for the operation of such a laser. Obviously, for a realistic setup we assume much too high a value for the atom-mode coupling g, which however seems justified as one of our individual atoms could represent 10^3 to 10^4 atoms in an experiment.

Interestingly, for the linewidth and shift properties, geometric effects are more important than they are for the average intensity. A square arrangement of the atoms creates a much larger shift than a triangular or a linear array, as can be seen in fig. 4.10. Note, that the increased shift with the atom number could lead to observable perturbations for larger ensembles. Again, operation at a lower pump intensity may help to minimize this effect.

4.4.2 Laser sensitivity to cavity length fluctuations

A central criterion for the stability of a laser is its sensitivity to fluctuations of the effective cavity length, which at present is one of the main limitations of reference oscillator stabilized lasers. Despite spectacular recent progress [1], comprehensive control at this level is still an extraordinary technical challenge. With the atoms acting as reference oscillators less effort in order to achieve technical stabilization is expected in an ideal superradiant laser. In the following we will study the effect of

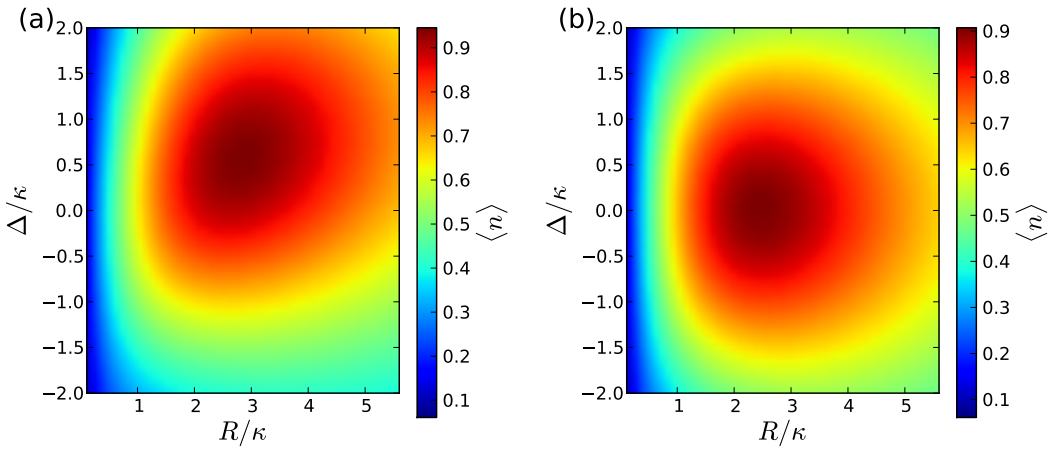

Figure 4.11: Average photon number for atoms on a square with $d = \lambda_0/10$ (left) and $d = \lambda_{magic}/2$ (right) for varying cavity detuning and an atomic decay rate $\Gamma = 0.2\kappa$.

a varying cavity frequency described by an effective detuning (Δ) on the average photon number fig. 4.11 and the frequency mismatch between the bare atomic transition frequency and the laser field ($\delta_a = \omega_0 - \omega_L$) as seen in fig. 4.12 depending on the average atomic distance. As shown in fig. 4.11(a) for closely positioned atoms the interaction evokes a significant blue shift of the cavity frequency, generating the maximum photon number. For atoms in a magic wavelength lattice, fig. 4.11(b), this shift is much smaller and close to the interaction-free case. The detuning sensitivity of the laser output spectrum to the detuning in these two cases is depicted in fig. 4.12, additionally the red line represents the threshold, where the inversion of the population begins. On the left-hand side of the red line, which is under the laser limit, the values of the detuning is rather imprecise.

We see that the laser frequency pulling via the cavity changes with the interaction and increases with the pumping and the intracavity photon number. Nevertheless, as indicated by the solid and dashed lines, the effective laser frequency change remains within an atomic linewidth even for cavity fluctuations on the order of the cavity width. At low pump strength and small inversion a sort of self-synchronization of the atomic dipoles via direct interactions can lead to very strong suppression of cavity fluctuations at the expense of very little output light, while for stronger pumping interaction effects are suppressed and the cavity drifts have a more significant impact on the laser frequency. Overall, we observe that by choosing optimal operating conditions a decoupling of the cavity fluctuations from the laser frequency can be suppressed very effectively, even in the case of atomic interactions. However, this

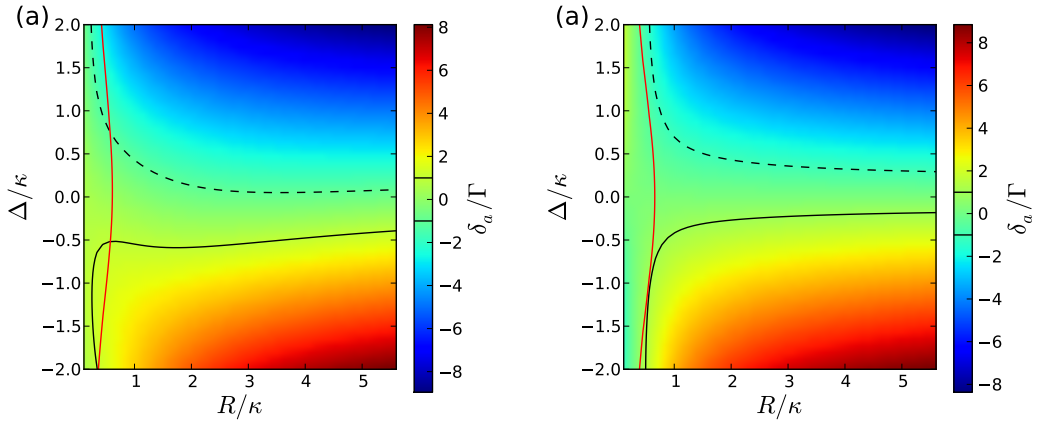

Figure 4.12: Frequency shift for a square atom configuration with $d = \lambda_0/10$ (left) and $d = \lambda_{magic}/2$ (right) for varying detuning and a fixed atomic decay rate of $\Gamma = 0.2\kappa$. The dashed line indicates $\delta_a/\Gamma = -1$ and the solid line corresponds to $\delta_a/\Gamma = 1$. The red line represent the laser threshold, $\langle\sigma_z\rangle = 0$, where to its right we are in the operating area of the laser.

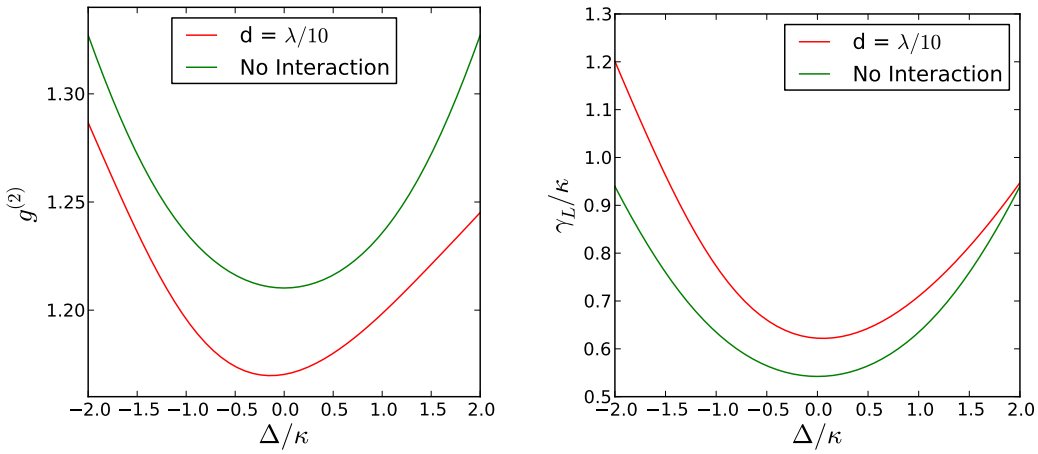

Figure 4.13: The dependency of the $g_2^{(0)}$-function (left) and the linewidth of the superradiant laser, γ_L/κ, (right) on possible length fluctuations of the cavity compared to the dipole-dipole interaction free laser.

decoupling generally also reduces the output power of the laser. In fig. 4.13 the two cases of strong an no interaction are compared directly. As expected, the interaction free case is absolutely symmetric in detuning. For strong interaction in a red detuned cavity the $g_2(0)$-function increase faster and the linewidth gets broader than for a blue one. Finally, we also recognize that for the strongly interacting regime the minimum is not at the position of the resonance.

Bibliography

[1] B. J. Bloom, T. L. Nicholson, J. R. Williams, S. L. Campbell, M. Bishof, X. Zhang, W. Zhang, S. L. Bromley, and J. Ye. An optical lattice clock with accuracy and stability at the 10-18 level. *Nature*, 2014.

[2] G.K. Campbell, A.D. Ludlow, S. Blatt, J.W. Thomsen, M.J. Martin, M.H.G. de Miranda, T. Zelevinsky, M.M. Boyd, J. Ye, S.A. Diddams, et al. The absolute frequency of the 87Sr optical clock transition. *Metrologia*, 45:539, 2008.

[3] R. H. Dicke. Coherence in Spontaneous Radiation Processes. *Phys. Rev.*, 93: 99–110, 1954. doi: 10.1103/PhysRev.93.99. URL `http://link.aps.org/doi/10.1103/PhysRev.93.99`.

[4] M. Gross and S. Haroche. Superradiance: An essay on the theory of collective spontaneous emission. *Physics Reports*, 93(5):301–396, 1982. ISSN 0370-1573. doi: 10.1016/0370-1573(82)90102-8. URL `http://www.sciencedirect.com/science/article/pii/0370157382901028`.

[5] F. Haake, M. I. Kolobov, C. Fabre, E. Giacobino, and S. Reynaud. Superradiant laser. *Physical review letters*, 71(7):995, 1993.

[6] K. Henschel, J. Majer, J. Schmiedmayer, and H. Ritsch. Cavity QED with an ultracold ensemble on a chip: Prospects for strong magnetic coupling at finite temperatures. *Physical Review A*, 82(3):033810, 2010.

[7] T. Maier, S. Kraemer, L. Ostermann, and H. Ritsch. A superradiant clock laser on a magicwavelength optical lattice. *ArXiv e-prints*, February 2014.

[8] D. Meiser, J. Ye, D. R. Carlson, and M. J. Holland. Prospects for a millihertz-linewidth laser. *Physical review letters*, 102(16):163601, 2009.

[9] L. Ostermann, H. Zoubi, and H. Ritsch. Cascaded collective decay in regular arrays of cold trapped atoms. *Opt. Express*, 20, 2012. ISSN 29634-29645.

[10] M. Takamoto, F.L. Hong, R. Higashi, and H. Katori. An optical lattice clock. *Nature*, 435(7040):321–324, 2005.

[11] H. Zoubi. Collective light emission of a finite-size atomic chain. *EPL (Europhysics Letters)*, 100(2):24002, 2012.

Chapter 5

Conclusions and outlook

By means of numerically solvable examples containing only few particles, we evaluated the influence of dipole-dipole interaction and collective spontaneous emission on radiative properties of a superradiant laser in a lattice geometry. In general, for fairly closely spaced atoms, shifts and frequency of the laser light uncertainties are of the order of the free space atomic linewidth. For very densely packed ensembles superradiant free space decay will substantially broaden the laser line. Quantitatively, various limiting cases can lead to a different scaling behavior of the photon number and linewidth or even to different photon statistics. Fortunately, for a Strontium setup based on a magic wavelength lattice, the detrimental effects remain very small, although they could attain an observable magnitude.

To improve the validity of the results of this work for larger systems, it would be necessary to simulate a higher number of atoms in a the different configuration, but to perform this calculations in a finite time we have to use extra approximations, for instance minimizing the Hilbert space by exploding its symmetries, recently, an $SU4$-approach was proposed, whereas the so-called truncated Wigner approximation might also be helpful. Another possibility for improvement is to use a different kind of numerical methodology, e.g. Monte Carlo wave function calculations.

With the possibility to simulate more atoms, it would be rather interesting to study a three-dimensional geometry, like a cube. In such geometries it might be feasible to vary the coupling constant between the field and the atoms, which simulates the standing wave mode profile. Furthermore, it would be worth looking at how different directions of the individual dipole moments influence the properties of the superradiant laser.

In this work we still assumed a rather ideal and to sum extent artificial pumping

mechanism. A more realistic pumping via extra levels or an injection of excited atoms would, of course, add extra noise and has to be designed very carefully. In any case, from the point of view of stability and shifts, the operation at weak pumping strengths seems favorable, although the very weak output field could be a technical challenge.

In the last years some experiments in the field of superradiant laser were conducted, a particularly prominent one is the realization with *Rb* by J. Thompson et. al., which operates as a Raman laser. The number of experiments will grow in the next years, e.g. F. Schreck, at the University of Amsterdam, plans to build a superradiant laser on an optical lattice.